NUCLEAR INSTRUMENTS AND METHODS 119 (1974) 61–89; © NORTH-HOLLAND PUBLISHING CO.

THE UNIVERSITY OF MICHIGAN CYCLOTRON FACILITY FOR RESEARCH IN NUCLEAR STRUCTURE*

W. C. PARKINSON, J. F. PETERSEN, R. H. DAY,
D. C. DuPLANTIS, W. S. GRAY and JOHN BARDWICK

Cyclotron Laboratory, Physics Department, The University of Michigan, Ann Arbor, Michigan 48105, U.S.A.

Received 12 March 1974

A number of improvements have been made in The University of Michigan 83″ sector focused cyclotron since its original construction. The reasons for the changes and the resulting improvement in the production of stable high-quality beams for nuclear research are described. A brief description of the total facility for research in nuclear structure is given.

1. Introduction

The scientific motivation, design criteria, and general features of The University of Michigan 83″ sector focused cyclotron facility were reported[1]) at the UCLA conference in 1962. Since that time a number of improvements have been made not only in the facility but particularly in the understanding and control of the essential elements for producing stable beams of ions of well defined energy and quality. The purpose of this paper is to give an update of the facility and in particular to detail the reasons for the changes that have been made since that early report.

Briefly, the detailed design and construction of The University of Michigan 83″ cyclotron facility was begun in 1960, and the first internal beam was obtained in late fall of 1962. It was designed to produce beams of protons, deuterons, ^{3}He, and alpha particles of energies 35 MeV, 40 MeV, 90 MeV, and 80 MeV, respectively, as well as a variety of heavier ions, and deliver these to a magnetic analysis system having a resolving power $E/\Delta E = 8 \times 10^3$ with an intensity and stability suitable for precision research in nuclear structure. These beams can also be delivered to an auxiliary beam line of resolving power 10^3 and are suitable for on-line charged-particle β and γ spectroscopy by time of flight, and for neutron cross section measurements. The specifications on beam quality for the high-resolution charged-particle system and the neutron time-of-flight spectrometer place stringent requirements on the stability of the magnetic fields (1:10^5) and dee voltage (1:10^4), on ion source brightness, and on extraction and external ion-optical systems. These are discussed in the following sections.

* Work supported in part by the U.S. Atomic Energy Commission.

TABLE 1

Design data for 83″ cyclotron.

Parameter	Value
Pole diameter	83″
Magnet weight	310 t steel 15.5 t copper
Yoke dimensions	224″ × 40″ × 83″
Yoke spacer dimensions	63″ × 40″ × 83″
Number of sectors	3
Hill gap	6.75″
Valley gap	11.0″
Shim gap (total)	1″
Pole lid thickness	3″
Extraction radius	36.5″
Maximum field rise with radius	2.2%
Maximum central field	19 kg
Central field for 40 MeV deuterons	14 kg
Conductor size	1.1″ × 1.0″ with 0.5″ diameter cooling hole
Total number of turns (12 pancakes)	336
Total resistance, 30 °C temperature rise	0.09 Ω
Maximum current	2000 A
Number of parallel water circuits	12
Length per water circuit	744′
Total flow at 160 psi (all pancakes)	47 gpm
Maximum current density	2220 A/in^2
Maximum operating temperature	180 °F
Magnet excitation	360 kW at 180 V

2. The magnetic field

2.1. THE MAGNET

The cyclotron magnet and vacuum chamber are as described previously[1]). The magnet (fig. 1) is of conventional H-type construction but has upper and lower pole tips 3″ thick separated from the upper and lower pole roots by a ½″ shim gap. The shim gap was originally intended to provide for shimming the

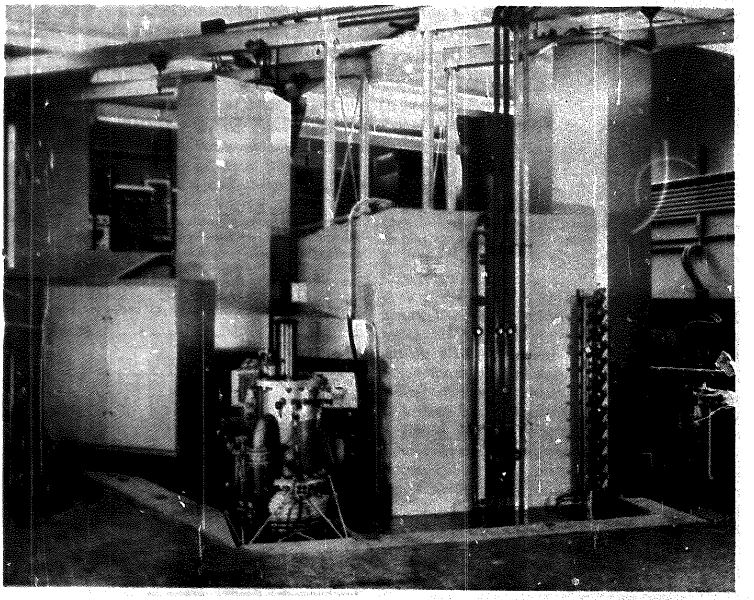

Fig. 1. View of the 83" cyclotron showing the main magnet and the 20" diffusion pump in the front center of the picture. The rf resonators or "silos" rise vertically, and the rf power amplifier cabinet is mounted to the left silo.

magnetic field to correct azimuthal harmonic components, but this proved to be unnecessary. Rose shims are now used in the gap at high magnet excitation to help shape the field and thus reduce the gradient coil power. It also provides a convenient mounting place for the sensor of the NMR magnetic field regulator. The parameters of the magnet are given in table 1. The three sets of spiral shims of contour shown in fig. 2 are mounted on the pole tips and terminate at a 12" radius. A transition region joins a central cone used to provide magnetic focusing. The shims produce a maximum flutter of 0.033 and provide axial focusing corresponding to $\nu_z \approx 0.15$ and acceptable radial stability. The main vacuum chamber is sealed to the magnet structure at a lip on the pole tips, and each tip is fastened to the pole root by six bolts, symmetrically located in groups of three on two different radii.

2.2. The gradient coils

To maintain isochronism for the accelerated particles, the average magnetic field must increase with radius, the increase for 40 MeV deuterons being approximately 2.2% or 330 G. The increase is obtained with twelve sets of circular trim or gradient coils attached to the inside surfaces of the pole tips and spiral shims. The inexpensive fabrication technique described previously[1]) has proved to be more than satisfactory. The measured contribution to the magnetic field from each set is shown in fig. 3.

2.3. The harmonic coils

Two sets of harmonic coils are provided to permit compensation of any residual equivalent first harmonic in the magnetic field and to provide a means of perturbing the ion orbits. The inner set extends from 3.5" to 12" in radius, and each pair of the set extends

85° in azimuth. Constructed of $\frac{1}{32}$" thick double-sided, 2 ounce copper-coated printed circuit board, they span the first $\nu_r = 1$ region where the field matches on to the isochronous value after coming off the central bump. The outer set extends from 42" to 50", and each pair extends 17° in azimuth (extraction radius is 36.56"). The coils are constructed of conventional water-cooled copper tubing. The currents in each of the three pairs of inner coils (identical currents in each member of a pair) can be varied sinusoidally about zero, with a 120° phase between each pair. Thus they give zero contribution to the average field while adding a first harmonic component that can be varied in amplitude and azimuthal phase. The currents in the outer set are varied sinusoidally about a dc base line.

2.4. Magnetic Field Measurements

The method and mechanism for mapping the magnetic field has been described previously[1]). The only modification for recent measurements was to rebuild the current regulator and voltage amplifier. The field of the magnet has been measured at excitations of 6, 12, 15 and 17 kG; the fields at 12 and 15 kG were measured for two different Rose shim geometries. In addition, gradient coil contributions to the main field were measured at 6, 12, and 15 kG.

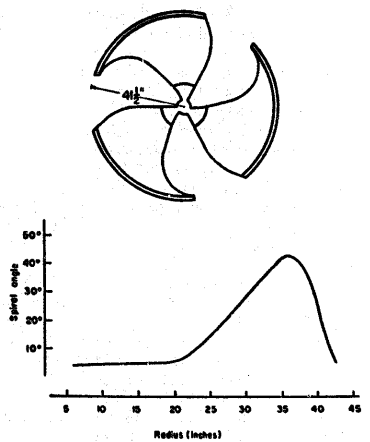

Fig. 2. Contour of the spiral shims (top) and the spiral angles as a function of radius (bottom).

The data were Fourier-analyzed to twelfth order in azimuth, and the results were tabulated versus radius. The numerical integration was done by a third-order quadrature routine and was accurate to ±0.1% in twelfth order. The analysis was carried out for all main magnet and gradient coil fields and is available both on magnetic tape for the PDP-15 on-line computer and in tabulated form. The accuracy of the final results is ±5 G with the main uncertainty being due to long-term drifts and mispositioning of the Hall probe. Recent measurements under vacuum indicated that a sligth differential flexing of the pole tips introduced a first harmonic component of 8 G. This was corrected by inserting six flat spacers between the pole roots and pole tips near the outer edge. The first harmonic amplitude is now everywhere less than 4 G.

Computer programs are available to predict for a given particle and final energy the main magnet excitation and gradient coil settings to produce the isochronous field. A particularly useful program computes the theoretical isochronous field and the field resulting from an input set of gradient coil currents. The two fields are then displayed graphically on the scope output of the computer. The final adjustment of the field is done using the circulating beam as described in section 5.7.

2.5. Power Supplies and Regulation

The stability limitations of the accelerated beam require that the total magnetic field be held constant to 1:10^5. Each of the component currents, those in the

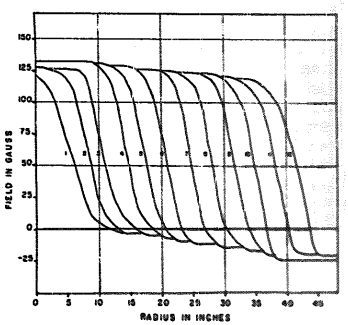

Fig. 3. The contribution of the twelve gradient coils to the magnetic field for current of 200 A at a main field excitation of 6 kG.

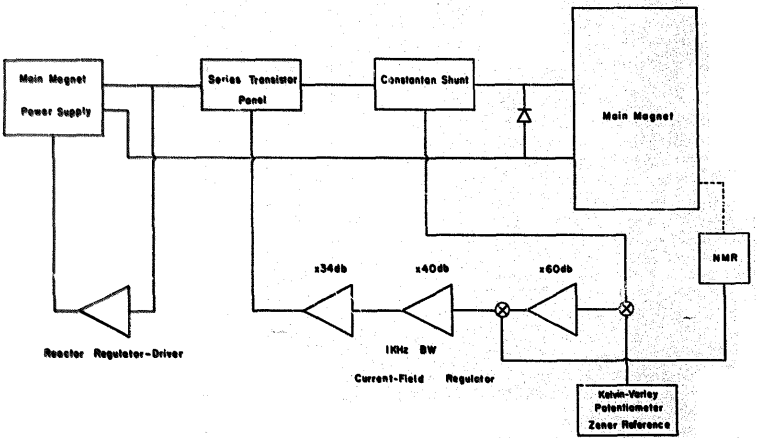

Fig. 4. Block diagram of the magnetic field regulator showing the current regulation loop for short-term stability and the NMR loop for both long-term stability and reproducibility of the magnetic field.

main field winding, the gradient coils and the harmonic coils, are individually regulated using series transistor banks as the control element. In addition, the total magnetic field is regulated using an NMR sensor located in the shim gap at a radius of 27".

The power supply for the main magnet is a silicon rectifier, saturable reactor-controlled unit rated for 180 V at 2000 A[1]). The field regulator has been modified and is now as shown in fig. 4. The system consists of two closed loops, one the reactor driver regulator and the other the current-field regulator. The reactor regulator controls the drive to the saturable reactors so as to maintain approximately 7 V across the series transistor panel. The drive power for the reactors is only 6 W at 1 A for maximum power output. Thus most of the gain is provided by the saturable reactors.

The current-field regulator uses current feedback for short-term stability and an NMR magnetic field sensor for long-term stability and reproducibility. The current sensor is a simple shunt constructed of sixteen constantan wires of diameter 0.128" and length 27" connected in parallel and enclosed in a rubber water jacket. The potential drop is 5 V at 2000 A; thus the maximum power dissipation in the shunt is 10 kW. Since the temperature coefficient of constantan is 2×10^{-6}/°C, a change of 5° would result in a current change of 1:10^5. Such changes are relatively slow and are negligible on a short-term basis. Thermoelectric potentials developed across the copper–constantan junctions in the shunt are cancelled by using opposing junctions in the voltage take-off leads.

The feedback signal from the magnetic field is produced by nuclear magnetic resonance. (An instrument manufactured by Varian Associates, in use for some years, is being replaced by a unit manufactured by Alpha Scientific.) The output provides the long-term reference signal to maintain the field constant despite thermal and hysteresis effects. The dc reference for the regulator is obtained from a temperature-regulated, Zener voltage supply and a commercial Kelvin–Varley potentiometer. The principal time constant of the magnet is $\tau = L/R = 10$ s. Shorter time constants associated with the aluminum dust covers around the coils and the saturable reactors are well within the response of the current loop. The regulator as shown in fig. 4 has a dc gain of 134 dB with a bandwidth of 1 kHz and is constructed using tube-type operational amplifiers. Because of its high gain–bandwidth product, the amplifier saturates from the 60 Hz noise pickup on the input. Rather than eliminating the pickup, use is

made of it by designing the regulator to operate on a proportional time modulation scheme. This produces a 4% modulation at 60 Hz of the magnet voltage, but because of the long time constant, the variation in magnetic field is less than $1:10^7$. The op-amps will soon be replaced with solid-state devices to obtain greater reliability. The regulator drives the transistor panel which is in series with the load. The panel consists of 210 power transistors (2N173) in parallel and mounted on water-cooled copper heat sinks. The 2N173 transistor is rated at 60 V (max.) and 150 W at 25°C. Thus the panel has a rating of 60 V and 31.5 kW, or approximately 10% of the maximum supply output. Each transistor has an emitter-balancing resistor and is individually fused so that failure of a single transistor does not interrupt operation.

A disadvantage of the single NMR sensor is that as the outer harmonic coils are varied in amplitude and phase the main field changes. This requires decoupling the regulator while changes are being made. To avoid this, a regulator is being constructed that uses as field sensors three Hall probes all at a radius of 30″ but located 120° apart in azimuth. By averaging the signals, the total field is held constant, independent of the harmonic component. Since long-term stability and reproducibility are the important requirements, critical components are maintained in a constant-temperature environment. An NMR sensor permits absolute field calibration; thus the 1% inherent non-linearity of the Hall plates poses no problem.

The Hall plates, type BN-701 manufactured by F. W. Bell, are driven by three floating constant-current supplies (nominally 100 mA), and the control currents are adjusted to match the output voltages to within the linearity tolerance. Each plate is in a temperature-regulated block held constant to within ± 0.01 °C. The voltage outputs of each are compensated by a resistor-thermistor network to partially cancel out the large temperature coefficient of the plates.

The resulting outputs are summed at the input of an Analog Devices model 260 K chopper-stabilized amplifier. With a net voltage of 200 mV at 10 kG, amplifier noise and drift contribute less than 2 ppm error. A commercial dc supply and divider network form the reference source. With a dc amplifier gain of over 100 dB, the overall sensitivity of the instrument is 4 V per 1 G field change.

The power supplies for the inner set of harmonic coils provide a first harmonic amplitude of 30 G for a current of 20 A. To avoid a shift in the baseline and to limit the power dissipation, bipolar power supplies are used about a zero average current baseline. For economic reasons, commercial unipolar power supplies were purchased and an SCR switching network was added. The proper amplitude for each supply is obtained from a three-cup sine pot, ganged 120° in phase. The three reference voltages pass through buffer amplifiers to provide the proper scaling for the voltage programming inputs of the Hewlett-Packard power supplies. A linear pot, on a shaft with the sine pots, supplies the proper quadrant information to a set of three dual comparators. The comparators are set so that an appropriate polarity signal is generated for each supply depending on the azimuthal setting of the pots. This signal switches on the proper pair of SCRs through a set of optically coupled SCR drivers. Additional circuitry assures that one pair of SCRs is switched off before the other is switched on.

3. The rf system

The rf system is perhaps unique in the isochronous cyclotron family in that it is a half-wave system and uses dee stem insulators. It was originally designed[1]) as a two-dee system with a single-sided, self-excited, tuned-grid, tuned-plate oscillator. In 1969 the oscillat

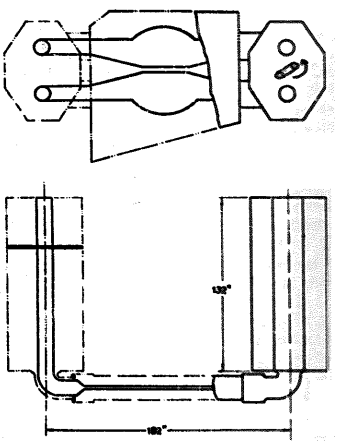

Fig. 5. Plan and elevation of the dee and resonator cavities. Coarse tuning of the resonators is done with sliding diaphragms, shown schematically in the resonator at the lower left. Fine tuning is done with the inductive tuning loop shown schematically in the resonator at the top right.

was replaced with a master-oscillator-power amplifier, and more recently (1972) the resonator was converted to a one-dee system. The reasons for these changes are detailed below.

The half-wave resonator system reduces the effective dee-to-ground capacitance by a factor of two; therefore the reactive current per dee stem is reduced by a factor of two and, other things being equal, the power loss is reduced by a factor of two. The use of insulators at the wall of the vacuum chamber simplifies the problem of mechanical support of the dees, which need not be cantilevered in the half-wave system, and essentially eliminates beam modulation due to mechanical vibration of the dees. Further electron multipacting is eliminated since the resonant line is in air rather than vacuum. However, multipacting of $^3He^{++}$ and $^4He^{++}$ has been observed in the center of the cyclotron near the ion tower. It is particularly troublesome at the dee voltages and operating frequencies corresponding to energies of $^3He^{++}$ and $^4He^{++}$ in the neighborhood of 45 MeV. The multipacting occurs when a relatively high gas pressure is used in the ion tower to increase the yield of doubly ionized He. It appears to be initiated by He^{++} ions extracted from the tower ionizing neutral He to He^{+} in the region just outside the tower.

The half-wave system has additional advantages: the voltage distribution along the dees is symmetrical about the center of the cyclotron which improves orbit stability by reducing the gap-crossing resonance; effects of thermal expansion are reduced; and because the rf resonators or "silos" are vertical as shown in fig. 1, the system occupies less floor space and permits access to all sides of the vacuum chamber. A plan and elevation view of the two-dee rf system is shown in fig. 5. In converting to a one-dee system, the dee facing the deflector and the two dee stems were simply removed.

The dimensions of the dee and resonator cavities are given on fig. 5. As originally designed, the frequency could be varied continuously from 6.5 to 15 MHz by means of the shorting diaphragms in each silo. After conversion to the one-dee system, the frequency limits fell to 5.7 MHz and 11.3 MHz. While the upper limit can be raised by making relatively minor mechanical changes, this has not yet been necessary. The diameter of the dee lines was chosen to limit the current density at the sliding contacts on the

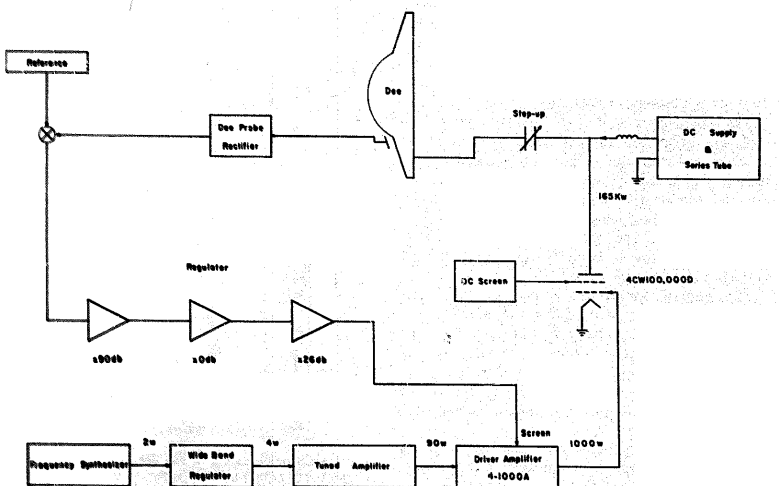

Fig. 6. Block diagram of the rf system showing the high-voltage power supply and series tube, the rf power amplifier chain, and the dee-voltage regulator loop.

diaphragms to 100 A/in. so that commercially available fingerstock could be used without the need for clamping or pressure devices. Fingerstock is also used at the connection of the dee to the resonator lines. The power inventory for the one-dee system is just half that given in ref. 1. Trimmer capacitors, mounted on each dee stem, are used for balancing the voltage distribution along the dee. Fine tuning of the resonator is done with an inductive tuning loop as described below. At the maximum design voltage of 70 kV peak dee-to-ground, the total rf power is ≈50 kW at 11 MHz. The calculated maximum electric field strength at the insulators is 15 kV/in., a reasonable value for alumina insulators available today.

At the time of the original design[1]) the dee stem insulators were considered the most critical elements in the entire system since they must withstand a high voltage, the power loss must be low to provide thermal stability, and they must withstand the mechanical stresses due to the vacuum load. The present insulators are Al_2O_3 in the form of discs 22" in diameter and 1½" thick with an 8" diameter central hole. They are placed parallel to the electric field lines in a nearly homogeneous field to prevent field lines crossing the surface. Water-cooled copper rings, mounted to the discs around the outer and inner circumferences by thermal setting epoxy, form part of the half-wave resonator line. The insulators are designed for 50 kV peak across a 5" spacing between inner and outer conductors. Because of the large diameter of the conductors, the field is nearly homogeneous and provides a factor of safety of about five in break-down to allow for irregularities in the electric field due to dust and sharp edges. The maximum rf power dissipated per insulator is about 600 W, which results in a temperature rise of 10°C. Limiting the insulator voltage to 50 kV peak limits the dee voltage at the center of the dee to 53 kV at 5.7 MHz and to 63 kV at 11 MHz. Over the years very little difficulty has been encountered with the insulators. The few losses that occurred in the early operation resulted from excitation of parasitic modes, since eliminated, or from accidental plating of carbon or copper onto them from misuse of the ion source. Under some conditions of thermal stress, possibly due to low water-cooling temperature, the epoxy bond separated sufficiently to allow a vacuum leak, but this has occurred too infrequently to be able to pinpoint the cause.

The reason for changing from the original self-excited power oscillator to an MOPA system was to improve the stability of both the frequency and the dee voltage. A block diagram of the rf system is shown in fig. 6. It consists of four major sections: the high-voltage power supply, the rf amplifier, the series tube regulator and switch, and the coupling loop to the resonator.

The power supply provides 17 A at 21 kV. As originally designed, it was a three-phase full-wave system using six vacuum diodes. The dc output voltage was varied and regulated by means of saturable reactors in the primary of the high-voltage transformer. Because of poor experience with the diodes (average life 1200 h at a cost of $180 per diode) and poor surge characteristics of saturable reactors, the vacuum diodes were replaced with six stacks of solid-state diodes, and the reactors removed. The diode stacks, manufactured by Westinghouse Electric Company, each consist of 88 type 1N1204A rectifiers in series, with a resistor-capacitor compensating network in parallel with each diode to suppress transients. Control of the output voltage is now obtained with a series tube (F-6379, plate dissipation 70 kW).

The series tube is used both for control and regulation of the dc plate voltage to the final amplifier tube and as a fast acting switch in the event of an arc in the resonator system. The on–off function of the series tube is accomplished with a solid-state logic control which is also used to control the dee-voltage regulator in the rf amplifier.

The rf amplifier, capable of delivering 165 kW of rf power to the resonator, is divided into three sections: the master oscillator, the intermediate amplifier-regulator, and the final power amplifier. The master oscillator is a General Radio coherent decade frequency synthesizer, type 1164-A6C. It delivers frequencies from 0.01 to 70 MHz with a stability of 2×10^{-7}/°C. Provisions are made for phase-locking to an external frequency standard for greater stability and for an external voltage control of the output frequency. This unit is located in the cyclotron control room and has sufficient output to drive the intermediate amplifier-regulator located in the cyclotron vault.

The two-stage intermediate amplifier-regulator provides the rf power necessary to drive the grid of the final power amplifier stage. The first stage is manually tuned while the second stage is tuned automatically. The autotuning is done with a phase-sensitive detector, a null detector with two-channel pulse output, and a translator to drive a dc stepping motor. Regulation of the dee voltage is accomplished by varying the screen grid voltage of the second stage (an Eimac 4-1000A) which in turn adjusts the drive delivered to the grid of the final power amplifier tube. Circuitry associated with the series tube is used to clamp the regulator output to

zero to prevent overdriving of the grid whenever there is an arc in the resonator system. The regulator output is also limited whenever a critical voltage or current level in the amplifier system is reached. This limiting scheme prevents most accidental damage from improper system operation.

The final power amplifier uses an Eimac 4CW100,000D operated in class C mode with a maximum power output of 165 kW. It is run with a fixed grid bias supply and a manually adjustable screen bias supply.

Power from the final amplifier is coupled to the resonator with a loop which uses a combination of inductive and capacitive coupling. (Pure inductive coupling could be used but is less flexible because the resonator is tuned by varying the length, hence the inductance, of the dee stems rather than by varying the characteristic impedance.) The amplifier cabinet is mounted directly to one of the silos as shown in fig. 1. The coupling loop consists of a variable vacuum capacitor (range 50–400 pF) connected between the amplifier plate and a movable tap point on the dee stem at the bottom of the silo. This arrangement permits the voltage ratio at the dee stem (V_d) to the amplifier plate (V_p) to be kept constant over the entire frequency range. The voltage ratio is to a good approximation $(V_d/V_p) = (L_1/L)\ (1+C_{pf}/C_s)$, where L_1 is the inductance from the tap to the shorting diaphragm of the resonator, L is the total inductance of the resonator, C_{pf} is the output capacitance of the amplifier, and C_s is the capacitance of the coupling capacitor. With an inductive step-up ratio of 1.2 at 6.5 MHz and 3.0 at 14 MHz and an effective amplifier capacitance of 175 pF, the coupling capacitance must vary from 60 pF at 6.5 MHz to 350 pF at 14 MHz. With $V_p = 14$ kV, the voltage at the center of the dee system can be maintained at 70 kV over the entire frequency range by varying the coupling capacitor. For the equivalent circuit shown in fig. 7, the step-up factor is $(V_d/V_p) = (C_{pf}+C_s)/C_s$.

In converting from the two-dee to one-dee system, the only change necessary in the rf system was an increase in the length, and thus the inductance, of the coupling loop. The increased inductance would have made it difficult to obtain the necessary step-up ratios at the higher operating frequencies. However, during the conversion the dee area was increased to provide for a uniform spacing at the accelerating gap (section 5.3), and the maximum resonant frequency of the system dropped to 11.3 MHz where the coupling length was not a problem.

The power amplifier uses a bridge balance neutralization scheme, but because of the low feed-back capacitance of the 4CW100,000D tetrode the adjustment is not critical. The more difficult problem is the excitation of harmonics modes. A troublesome cross-over mode exists due to the step-up capacitor and the inductance of the length of dee stem from the coupling point to the shorting diaphragm. Thus when the frequency is changed, the rf plate waveform must be monitored for harmonics while the step-up capacitor is adjusted to the proper dee voltage range. Because of the wide power range of the amplifier, however, loading and step-up ratio adjustments are not critical and can be varied to avoid the crossovers.

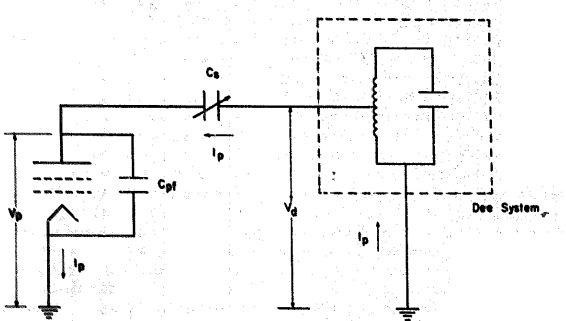

Fig. 7. Equivalent circuit of the rf power amplifier output stage coupled to the dee system. The voltage step-up factor is $(V_d/V_p) = (C_{pf}+C_s)/C_s$.

Tuning the rf system is straightforward. The synthesizer, the first and second stage tuning controls, and the shorting diaphragms are set to their proper position as read from graphs. With low power applied, the waveform is observed for harmonics as the step-up capacitor is changed. If necessary, small changes are made in the capacitor value to eliminate the harmonics. With a little experience, even the novice operator can tune the system.

The proper centering of the particle orbits requires that the rf voltage distribution along the dee be symmetrical about the dee center. The unbalance caused by a change in the step-up capacitor is compensated by means of a variable capacitor, symmetrically located on the companion dee stem.

Coarse tuning of the resonator is done with the two movable shorting diaphragms. Since the resonator has Q greater than 600 under full load, to maintain the dee voltage constant to 1:10^4 over long periods requires that the resonator be fine-tuned to compensate for changes in mechanical dimensions due to thermal effects. This is done by means of an inductive loop located between the dee stem and the ground sheet at the bottom of the south silo as indicated in fig. 5. The loop is formed from 1″ diameter copper pipe into a 14″ × 14″ square. By rotating the loop about an axis parallel to the dee stem, the characteristic impedance of the line can be altered and the resonant frequency adjusted to the frequency of the master oscillator. This additional variable inductive coupling produces a total change of 5 kHz at 8 MHz. The loop is rotated automatically by a synchronous dc stepping motor working in conjunction with a phase detector on the grid and plate voltages of the final amplifier tube.

The dee voltage is monitored and metered using guard-ring capacitive pick-offs mounted on the north and south silos of the resonator. A half-wave rectifier followed by a low-pass filter produces a dc signal proportional to the amplitude of the rf voltages on each end of the dee. The pick-offs drive read-outs on the control console, and the difference voltage drives a dee balance read-out. A third capacitive pick-off provides an isolated reference signal for the dee voltage regulator.

The stability requirement of 1:10^4 for dee-voltage regulation is difficult to achieve in a large resonator. In addition to the modulation expected from the power line, other sources have been identified. These include high-frequency (10–20 kHz) amplitude modulations due to the frequency synthesizer, discrete resonant frequency changes due to the stepping motor, and effects caused by acoustical noise flexing the resonator. The high-frequency modulations were reduced by a wideband regulator on the output of the synthesizer while the effects produced by the others were within the bandpass of the dee regulator.

The short-term stability is monitored by observing the output of one of the dee meter pickup probes on a Tektronix type 1A7 oscilloscope preamp. With a dc output of typically 10 V, observed variations are less than 1 mV peak to peak. The measurement of both short- and long-term instabilities is discussed in section 5.8 where the general question of beam stability is discussed.

4. The ion source problem

In a high-resolution charged-particle experiment the practical limit on resolution is often set by the magnitude and quality of the current available in the scattering chamber, and this in turn is limited by the brightness of the effective source provided by the cyclotron. The brightness of the cyclotron source is determined by the quality of the ion-optics internal to the cyclotron and/or the brightness of the ion source itself. The quality of the internal ion-optics is discussed in a subsequent section; some of the limitations on the source brightness and on the magnitude of the circulating beam are discussed here.

The ion source used at present is an Oak Ridge hot-filament hooded-arc type[2]) with the anode at ground potential and the filament negative with respect to ground. The filament is formed into a U-shape from $\frac{1}{8}$″ diameter tungsten rod and is heated with dc power (400 A at 4 V). A small notch ground into the tungsten directly under the $\frac{1}{8}$″ diameter hole at the bottom of the anode column ensures that the highest temperature, and therefore the maximum thermionic emission, occurs in line with and directly under the anode column. The anode column is $2\frac{9}{16}$″ high by $\frac{1}{4}$″ diameter and has a reflecting button of tantalum at the top insulated from the tower by a boron nitride insulator. A tungsten shield just below the filament prevents a discharge from the filament to the bottom of the filament chamber. The gas discharge is operated in the positive incremental-resistance abnormal-glow region of the voltage-current characteristics rather than in the negative-resistance arc-discharge region. Either the anode (discharge) current or the anode-cathode voltage may be regulated, and thus the discharge can be operated in either a current-regulated or voltage-regulated mode. The power supply consists of two commercial silicon controlled rectifiers in series to provide a total of 600 V at 8 A. Under proper condi-

tions of gas pressure (a flow through the tower slit of 2 cm³/min for deuterium and 4–5 cm³/min for helium) and with current-mode regulation, good arc stability is obtained.

The width of the slits in the tower and puller are varied according to the ions to be accelerated and the desired quality of the beam. Nominal dimensions for hydrogen and deuterium are 0.020″ and ½″ high for both tower and puller slits, and 0.040″ and 0.020″ for tower and puller, respectively, for $^3He^{++}$ and $^4He^{++}$. For heavy ions such as $^{12}C^{4+}$, the slits are typically opened a factor of three or four wider. The tower-to-puller spacing is nominally 0.300″. The current injected into the dee is optimized from the control console by moving the filament to align the discharge in the tower and by "rolling" the tower to bring the discharge tangent to the tower slit.

The number of positive ions available for extraction from the ion plasma depends on the operating conditions of the gas discharge[3]. For high ion density in the plasma, the current extracted is space-charge limited (temperature-saturated), while for low ion densities the current is temperature-limited (voltage-saturated), analogous to temperature-limited current in a thermionic electron tube. (The data in fig. 3 of ref. 2 indicate the onset of voltage saturation near 10 kV anode potential.) It is well known among cyclotron operators that the beam current depends on optimizing the ion source conditions, that is, optimizing the gas discharge (gas pressure, anode voltage and current), and the geometry (tower "roll" and tower-puller alignment). However, this does not necessarily optimize the brightness. [We define the brightness B of a source as the energy per unit time per unit area per unit solid angle, or $B = Ip^4/(2mNA_xA_z)$, where I is the current, p the momentum, N the charge state, and A_x and A_z the areas in phase space.]

The current extracted from the plasma and injected into the dee through the puller may be expressed in the form $I_b = KV_d^{\alpha}$, where K is a constant, and V_d is the rf dee voltage. For deuterons the value of α is found to vary[3] from 1.42 to 1.58, and for $^3He^{++}$ α varies from 1.20 to 1.35. For a plane-parallel geometry, the space-charge limited current should vary as $V_d^{\frac{3}{2}}/d^2$ (Childs' Law), where V_d is the dee potential and d the separation of the electrodes. Thus the data agree as well as expected with Childs' Law over the range of measured currents, particularly since the initial conditions at the cathode must depend on the condition of the plasma. It is interesting to note that for some twenty-two commercial thermionic diodes the value of α was found to vary[4] over the range of 1.24 to 1.49.

The fact that the current is space-charge limited emphasizes the importance of maximizing the charge density of the desired ion species. For an ion species of charge q_i, mass m_i, and permittivity ε_0, the current density given by Childs' Law is

$$J = \tfrac{4}{9}(2q_i/m_i)^{\frac{1}{2}}\,\varepsilon_0 V^{\frac{3}{2}}/d^2 \text{ A/m}^2,$$

in MKS units. A convenient expression is

$$J = 2.66\left[\frac{N_i}{A_i}\right]^{\frac{1}{2}}\frac{V^{\frac{3}{2}}}{d^2} \text{ A/m}^2.$$

In the last expression V is in kV, d is in inches, N_i is the charge state, and A_i is the nuclear mass number. It can be shown[3]) that for a mixture of charge states in the plasma, the current density of any one of the species is

$$J_1 = \tfrac{4}{9}\varepsilon_0\,\frac{(2q_1/m_1)^{\frac{1}{2}}}{\left[1+\sum_{i=2}^{k} n_i q_i/(n_1 q_1)\right]}\cdot\frac{V^{\frac{3}{2}}}{d^2},$$

where n_i is the number density in the plasma of ions of species i. (This follows from the fact that div $J_i + \partial\rho_i/\partial t = 0$ for each ion species i.) Under the normal conditions of operation of our present source, the observed current of $^3He^{++}$ is a factor of fifty lower than expected and corresponds to a relative population of $^3He^{++}$ to $^3He^+$ in the plasma of about 2%. This is consistent with the measurements of yields of hooded-type arc sources by Papineau et al.[5]). It is also noted that because of their low ionization potential, a small amount of impurity gas, particularly H, D, or O, "poisons" the arc by effectively preventing multiple ionization. For D_1^+ the yield is reduced by a factor of five because of the presence of the molecular ions D_2^+ and D_3^+. (While the D_3^+ ions would be accelerated on the third subharmonic, they are blocked by slits in the central geometry.) Again this is consistent with the measurement of Papineau et al. of 1:2:1.5.

The limitations of the hot-filament type ion source for the production of heavy ions of high charge states is well kown, and much effort has been spent on the development of suitable sources[6]). A source similar in design to the PIG source in use at Oak Ridge[7]) is now under test here, the principal modification being that the diameter of the cold cathodes is ⅛″ rather than ⅜″. The ionization density of a given charge state, other things being equal, is proportional to the current density in the discharge. The ions of higher charge states are concentrated in the central zone of the plasma and are therefore shielded from external electric fields by the outer space charge. By reducing the cathode diameter, hence the total current and power

for the same current density, the central zone can be placed closer to the extraction slit. The net result is expected to be the same yield of a given charge state but with a factor of nine reduction in required power. The results of tests will be reported separately.

The gated ion source, developed for use in time-of-flight measurements with either type of ion source, has been described previously[5]. It uses a tetrode geometry, gives 100% gating efficiency for all ions, and may be operated at any multiple of the rf period. Its use in beam diagnostics is discussed in section 5.7.

Measurements of the emittance and luminosity of ion sources have been reported by Mallory and Blosser[8]. (Brightness and luminosity are related as $B = LE/q$.) The information given on their ion source geometry is not sufficient to determine if the current is space-charge limited, but the numbers are consistent with what one expects. The differences in the current yields for the large and small tower diameters are also consistent with a temperature limitation and a space-charge limitation. Thus the significance of their data is not clear. Any attempt to improve the brightness or emittance will ultimately be limited by space-charge effects.

Another well known limitation on the circulating beam is axial blow-up due to space charge at a radius corresponding to the minimum frequency of the axial oscillation ν_z. The qualitative effects have been discussed by Welton and by Reiser, and a number of calculations have been made[9]. They are generally in good agreement with measurements on a variety of cyclotrons. The result expressed in MKS units is

$$I = h\varepsilon_0 \nu_z^2 (\Delta\phi/2\pi)(\Delta E/q)\omega \text{ A},$$

where h is the aperture or height of the dee, $(\Delta\phi/2\pi)$ is the azimuthal extent of the beam (the duty cycle), $(\Delta E/q)$ is the energy gain per turn expressed in eV, ε_0 is the dielectric constant for free space, and ω is the angular frequency of the rf. For the University of Michigan cyclotron, for example, the minimum value of $\nu_z \approx 0.15$ occurs at a radius of about 8", corresponding to $E_{max}/20$. For the dee aperture of $h = 3\times10^{-2}$ m, an energy gain per turn of 100 keV, and $\omega \approx 50\times10^6$, the space-charge limited current is of the order of $40(\Delta\phi/2\pi)$ mA, which for a duty cycle $(\Delta\phi/2\pi)$ of 1/50, ($\approx 7°$ phase width) is about 800 μA. If the duty cycle is 1/10 (36° phase width), the limit is 4 mA. For reasons discussed in section 5.4, a phase width larger than 7°–10° does not increase the useful current through an external ion-optical system of high resolving power. (It might be noted that flat-topping the rf circumvents this limitation and promises an order of magnitude improvement not only in the time structure but also in the useful current.)

In general, for the geometry and conditions of operation in our cyclotron when producing a high-quality beam, it is the tower-puller space charge that limits the circulating beam rather than axial blow-up. For example, for deuterons with 7° phase width the axial limit is about 800 μA, while for the same phase width and slits of area 6×10^{-6} m^2, the current would be about 880 μA for pure D_1^+ but is reduced to about 180 μA due to the presence of the other ion species. This is further reduced another factor of five on the first half turn to obtain the necessary radial divergence. The measured axial extent of the beam, as shown by burn patterns (fig. 17), is consistent with these conclusions.

5. Orbit dynamics and beam diagnostics

5.1. Introduction

The understanding of the isochronous cyclotron began with the original paper of Thomas[10]. Since that time the literature on both theory and practice has become extensive[11], and it is correct to say that the understanding is now essentially complete.

Using the theory as a basis, an extensive study has been made of the many parameters affecting the quality of the internal and extracted beam in The University of Michigan cyclotron, and modifications have been made where necessary to permit control of these parameters. While many interdependent variables and effects are involved, it is possible to discuss several important areas independently. To facilitate later discussion a brief summary is given of the principal equations governing the ion motion.

The basic equation of the cyclotron results from the equality of the Lorentz force and the centripetal force, namely

$$Bqv = mv^2/R, \tag{1}$$

from which it follows that for an ion accelerated to relativistic velocities, the period of rotation is

$$T = \frac{2\pi}{qB}\frac{m_0}{(1-v^2/c^2)^{\frac{1}{2}}}. \tag{2}$$

Thus if the frequency is to remain fixed, the magnetic field must increase with radius to compensate for the relativistic increase in mass. The conditions for stability of the ion motion in the axial direction are met by introducing an azimuthally varying component in the magnetic field $B_z(\theta) \approx B_0[1 + f\cos(N\theta)]$ to obtain contributions to the axial force. These are the Thomas

effect[10]) ($v_r \times B_\theta$), the Laslett effect[12]) ($v_\theta \times B_r$), and the Kerst effect[12]) arising from a $z(\partial B_r/\partial z)$ term. The vertical oscillation frequency, ω_z, resulting from a geometry of N sectors of flutter f and spiral angle γ is to first order

$$\omega_z = \omega_0\left[-k + \frac{N^2}{N^2-1}\frac{f^2}{2}(1+2\tan^2\gamma)\right], \quad (3)$$

where $\omega_0 = qB/m$ and $k = (\mathrm{d}\langle B\rangle/\langle B\rangle)/(\mathrm{d}r/r)$ are defined with respect to the azimuthally average field over the scalloped path. The first-order radial oscillation frequency is $\omega_r = \omega_0(1-n)^{\frac{1}{2}}$, when $n = -(r/B_z)(\partial B_z/\partial r)$. The energies of the ions accelerated in the 83" cyclotron require n (or $-k$) to be $n \approx -0.04$, thus $\omega_r \approx 1.02\omega_0$. The parameters in eq. (3) for the three-sector symmetry result in $\omega_z \approx 0.14\omega_0$. If the magnetic field is written as a Fourier series, namely

$$B = B_0[1 + \sum_{m=1}^{\infty} f_m \cos(m\theta + \psi_m)], \quad (4)$$

then the equilibrium radius R_e can be written as

$$R_e = R_0[1 + \sum_{m=1}^{\infty} \frac{f_m}{(1-n)-m^2}\cos(m\theta + \psi_m)], \quad (5)$$

where it is assumed that $\theta = \omega_0 t$, and $R_0 = mv/B_0 q$. The radial momentum p_R can be found by simply evaluating

$$p_R = m\frac{\mathrm{d}R_e}{\mathrm{d}t}, \quad (6)$$

where θ is replaced by $\omega_0 t$ for purposes of differentiation. For the 83" cyclotron the dominant term in eqs. (4) and (5) is $m = 3$. Eq. (5) indicates that a resonance exists for an azimuthal first-harmonic force ($m = 1$) when $n = 1$. When $n \neq 1$ but is near 1, as it must be in low-energy cyclotrons, the ion orbits are still sensitive to a first harmonic. Such a force may be due to a first-harmonic component in the magnetic field. It may also arise from a net 180° asymmetry in the electrical forces applied to the ion during the course of one accelerating cycle.

The circulating ions are accelerated only during a small fraction of the rf cycle so that the phase width expressed in terms of rf degrees is narrow. At each dee to ground gap crossing the energy gain is

$$\Delta E = qV\cos\theta, \quad (7)$$

where q is the ion charge, V is the dee voltage, and θ is the phase angle with respect to the peak rf voltage. The turn spacing ΔR between successive orbits at a given azimuth is

$$\Delta R = \frac{1}{\omega}\left\{\left[\frac{2}{m}(E_n + 2qV\cos\theta)\right]^{\frac{1}{2}} - \left(\frac{2E_n}{m}\right)^{\frac{1}{2}}\right\}, \quad (8)$$

where E_n is the ion energy after n complete turns. The turn spacing decreases as the energy and radius increase such that, assuming that the phase remains fixed, the product $R\Delta R = \Delta E/m\omega^2$ is a constant. For a beam making 200 turns to extraction, the turn spacing decreases from 1 cm at a radius of 20 cm to 0.218 cm at extraction (92 cm).

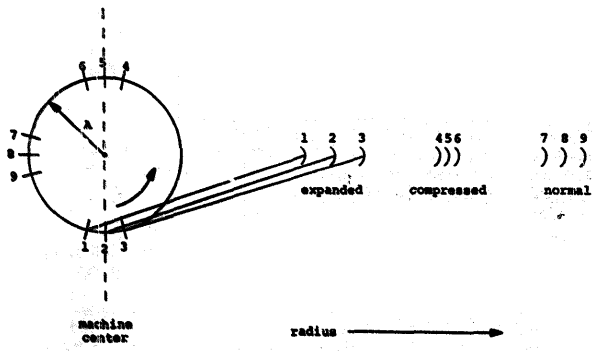

Fig. 8. An illustration of the turn-spacing modulation. See text for description.

The normal acceleration process results in a progression of orbits which oscillate with small amplitude about the equilibrium trajectory. From eq. (5) it is clear that large radial oscillations can be induced by first harmonic forces. Oscillations will also result if the ions do not start from the central region with the proper initial conditions. In either case it is useful to consider the motion when a sizeable amplitude is present. The ions will oscillate about the equilibrium trajectory R_e [eq. (5)] at the frequency ω_r with amplitude A and phase ϕ. The resulting expression for the radius R is

$$R = R_e + A\cos[(1-n)^{\frac{1}{2}}\theta + \psi]. \quad (9)$$

If the current density is observed as a function of radius at some fixed azimuth, the normal turn spacing ($R\Delta R$ = constant) will be modulated. The effect is illustrated in fig. 8. Neglecting the scalloping of the equilibrium trajectory, successive orbits can be approximately described as circles whose centers precess about the center of the field at the rate per turn of ω_p/ω_0, where $\omega_p = \omega_r = \omega_0$. For example, if $\omega_r = 1.02\,\omega_0$, the resulting modulation of the normal turn spacing will have a period of 50 turns. The circle described by the orbit centers will have a radius A which can be identified as the amplitude of the radial oscillation. Depending on the location on this circle (the phase of the precession), the normal turn spacing observed at some azimuth may be expanded (orbits 1, 2, 3), compressed (orbits 4, 5, 6), or essentially unchanged (orbits 7, 8, 9). Clearly if A is large enough, the turn spacing may become zero or negative at some radii corresponding to the well known types of cycloidal motion[13]). The amplitude A can be determined from the turn pattern from the expression

$$A = \frac{N}{4\pi}\left[(\Delta R_{max} - \Delta R_{min}) - \Delta R_1\left(\frac{R_1}{R_2} - 1\right)\right], \quad (10)$$

where N is the number of turns per precessional period, R_1 and R_2 are the radii of minimum and maximum turn separation, respectively, and ΔR is the separation between adjacent turns. The phase of the modulation or the position of the maxima and minima will depend on where in the acceleration process the radial oscillation was excited. As an example, one common cause of a sizeable oscillation amplitude is a mispositioning of the ion source along the dee gap centerline. If the tower is at too large a radius, a particular phase of the precessional motion will result on the nth turn at the azimuth of the probe. If now the tower is moved to too small a radius, a phase shift of 180° will be observed on the same nth turn and azimuth. This effect provides a powerful diagnostic technique.

Any complete understanding of the ion orbits must include an understanding of finite width, and variation in width, of the individual turns. The emittance of each pulse of ions extracted from the source will be limited by the geometry of the central region. The narrow tower

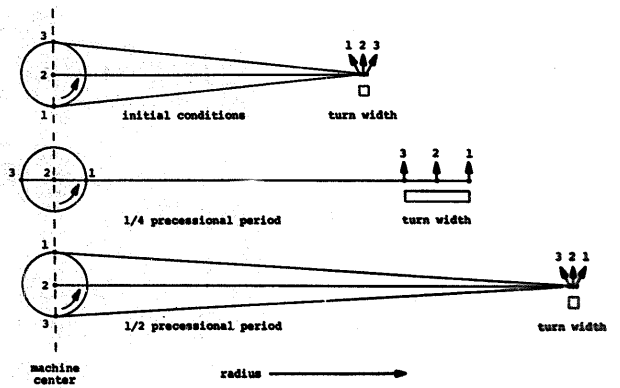

Fig. 9. An illustration showing the turn-width modulation. See text for description.

slit defines the initial radial and axial position, and the puller or other slits will determine the radial and axial divergence. The consequence of the divergence is illustrated in fig. 9. At the top, three ions are emitted from a narrow radial source in the three directions shown, each with its instantaneous center as shown at the left. For purposes of this illustration, ion number 2 is chosen to be on the equilibrium orbit. The trajectories of 1 and 3 are thus off-center and as they are accelerated will undergo the cycloidal motion described above. The effect of the divergence on the turn width is demonstrated by the two lower figures. After one-quarter of the precessional period, the turn width observed at a given azimuth will be wider; after one-half a period, the width will again correspond to the original width. Thus the turn width will be modulated at exactly twice the precession frequency, thus at exactly twice the frequency of the turn spacing modulation.

The significant point about the radial motion is that the two modulations, the turn spacing and the turn width, are initiated independently. The first, which in effect is a miscentering of the entire pulse, may be caused either by improper central-region conditions and/or by first harmonic forces at any radius and can result in any arbitrary phase of the precession at the nth turn and azimuth. The second, due to the finite divergence and width of the source, has a definite initial phase; thus the precessional phase at the nth turn and azimuth depends only on the integrated value of ω_r and the number of turns. Both have the same frequency ω_r so once initiated they remain fixed in relative phase. Examples of turn patterns illustrating these effects are given later.

5.2. Diagnostic instrumentation

The four principal pieces of diagnostic equipment used in measuring the properties of the beam are the "centerline" probe, the "burn pattern" probe, the phase probe, and the emittance "snooper".

The centerline probe measures current and current density as a function of radius. As originally designed, it moved in radius along the centerline between the two dees. With the one-dee configuration, however, as shown in fig. 11b, it moves parallel to but displaced 2¼" from the centerline of the dee and dummy dee and thus does not move along a true radius. Its azimuthal position tracks nearly along the center of a hill. The probe, shown in fig. 10, is 2" in diameter and carries an electrically insulated water-cooled copper head lined with carbon. A tungsten wire probe, the diameter of which can be changed, is mounted on a separate insulated shaft and can be retracted inside the probe head or extended up to 1½" from the head toward smaller radii. Both fill the vertical aperture of the dee. Current leads from the head and the wire, after filtering the rf, are brought to meters and to a strip-chart recorder in the control room. A positive potential of up to 100 V is inserted in series to collect secondary electrons. The probe mechanism provides an accurate read-out of the radial position which can also be recorded on the strip-chart.

The burn pattern probe, shown in fig. 10, carries a frame in which are mounted thin Mylar sheets for exposure to the beam. The thickness of the Mylar is

Fig. 10. The current and current-density probe (centerline probe) is shown at the left and the burn-pattern probe at the right. The tungsten wire, shown extended from the carbon-lined head of the centerline probe, can be retracted into a slot in the head.

varied depending on the energy and charge state of the circulating beam. The phase probe is a γ-ray time-of-flight system[14]. The phase and phase width of the circulating beam are measured, for example, by measuring the time interval between a fixed reference point of the rf cycle and the arrival of γ-rays emitted when the beam strikes the centerline probe. It consists of a small fast plastic scintillator coupled to an RCA8575 phototube and Ortec 270 constant fraction timing base which provides a start signal to an Ortec 437A time-to-amplitude (TAC) converter. The stop signal accurately synchronized with the rf is manufactured from a signal obtained from a capacitive pick-off on the dee line. The time resolution of the system is about 350 ps. The probe head can be moved to various locations in the cyclotron vault, or along the

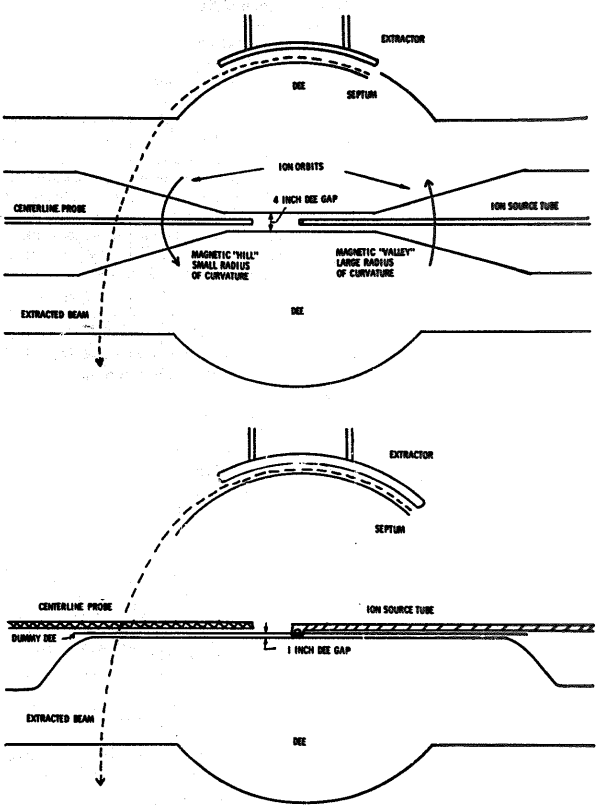

Fig. 11. The two-dee configuration (top) and the one-dee configuration (bottom).

beam lines, to measure the time width of the beam at any point.

The emittance snooper makes use of the slotted-plate technique[15]). A carbon plate containing ten vertical slits 0.010" wide and spaced 0.250" can be rotated into the external beam path. At a distance 96" downstream a wire probe 0.010" in diameter can be moved across the beam. The position of and the current to the probe are plotted on an x–y recorder at the console. Thus the emittance can be measured routinely in a few seconds time.

5.3. Orbit centering

The cyclotron was designed to provide beams of high quality to a high-resolution charged-particle spectrometer and to a time-of-flight spectrometer. To meet the time-of-flight requirements, single-turn extraction is essential. To achieve single-turn extraction, the individual orbits at the septum must be radially well defined and well separated, which implies no precessional mixing and therefore a narrow phase width. The two characteristics, separation and width, are related in that they both are influenced by the radial restoring force, but it has been shown that to a large extent they can be treated as separate problems. For non-centered orbits large turn spacings may be obtained during portions of the precessional period, but to make use of this the phase of the precession at the septum must be carefully controlled. The turn width also varies throughout the precessional period.

In principle it is possible to arrange for the relative and arbitrary phase of the two effects to be such that the two conditions are met simultaneously. In practice, however, the fine details of the first harmonic components of the magnetic and electric forces are not well enough known. Thus to make single-turn extraction feasible, one of the two effects must be eliminated. The turn width or divergence can be easily controlled by slits but only at a large sacrifice in intensity. The other possibility is to center the orbits and rely on the natural turn spacing at the septum. The turn width can then be controlled by varying the precessional phase without changing the turn spacing. This is the procedure that has proven most fruitful with our cyclotron. In this mode of operation, the natural turn spacing at the septum is determined by the number of turns, and therefore the dee voltage. This effectively places an upper limit on beam energies available for time-of-flight measurements. At present this limit corresponds to 250 turns, which for ^{3}He is 50 MeV.

As is well known, the central geometry is crucial to obtaining centered orbits. The geometry, shown in fig. 12, is such that the assumption of an impulsive energy gain every 180° is a reasonably good one. Thus for later orbits to be centered, the ion source must be offset[16]) from the magnetic field center along the dee line by an amount $R = 0.75R_1$, where R_1 is the radius of curvature of the first half turn, namely

$$R_1 = \frac{7.2}{f}\left(\frac{VN}{A}\right)^{\frac{1}{2}} \text{cm}, \tag{11}$$

where f is the rf frequency in MHz, V is the dee voltage in kV, N is the ion charge state, and A is the atomic mass. While this simple expression for the offset is based on the impulse approximation and the assumption of a uniform magnetic field, it is in good agreement with a more detailed analysis described below.

The nature of the radial restoring force in an isochronous cyclotron is such that the ion orbits are particularly sensitive to electric or magnetic first

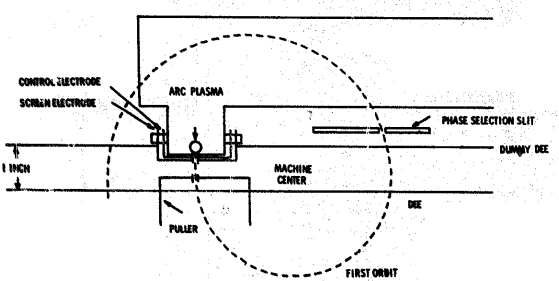

Fig. 12. The central-region geometry.

harmonic forces. In the original construction the cyclotron used two dees, operating in a push–pull mode with the dee geometry as shown in fig. 11a. This geometry in conjunction with the threefold symmetry of the flutter in the magnetic field was shown to produce a significant first harmonic force at large radii. The origin of this force results from the fact that the ion crosses each of the four effective dee to ground gaps at an angle while the electric field is perpendicular to the dee aperture[17]). The ion trajectory at each crossing can be found approximately from eq. (5) and the force resolved into tangential and normal components. The net formal force for a complete revolution was found to be equivalent to a magnetic first harmonic of about 10 G. From computer studies it was known that first harmonics of this magnitude would have serious effects on orbit centering. The problem was eliminated when the cyclotron was converted from a two-dee to a one-dee system. While the primary reason for the conversion, the elimination of the rf voltage in the extraction channel, is discussed below, it is worth noting here that the new geometry, shown in fig. 11b, permits a much smaller dee gap at all radii since it is no longer necessary for the ion source tube to be centered in the gap. Thus there are only two gap crossings per turn at all radii and the net equivalent first harmonic is well within acceptable limits.

A commonly used measure of the quality of centering is the radial phase-space plot. In the threefold symmetry of the cyclotron's magnetic field, in the absence of acceleration, an ion will have the same radius and same radial momentum components every 120° in azimuth if it is perfectly centered [eq. (5)]. An uncentered orbit describes an ellipse in phase space which precesses about the equilibrium orbit with frequency $\omega_p = \omega_0[1-(1-n)^{\frac{1}{2}}]$. Fig. 13 is a plot for a deuteron beam of final energy 40 MeV computed at a radius of 20.351". The plot closes on itself after 62 turns and the ellipse precesses in the direction of beam rotation as expected from eq. (9). It was drawn from the output of the computer program EORB used to find equilibrium orbits for a beam of given energy as a function of the magnetic field. It is one version of a more general program ORBIT written to solve the two-dimensional equations of motion for the beam in the median plane. The inputs to the program include the median plane electric field, measured using the electrolytic paper technique, and the Fourier components of the measured magnetic field including the contributions due to the gradient coils. Using a Runge–Kutta integration routine, the program numerically integrates the coupled radial and azimuthal equations of motion. After the first half turn, the energy gain is assumed to be impulsive at each dee crossing.

Imposing the constraint that the beam be centered at extraction implies that the beam be undergoing a radial oscillation at smaller radii, with the amplitude of the oscillation increasing monotonically toward the center. It is necessary, therefore, as indicated above, that the initial trajectory of an ion leaving the ion source be such as to develop into a centered orbit when

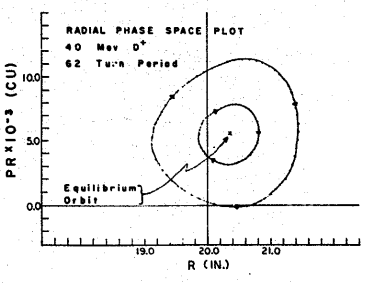

Fig. 13. A radial phase-space plot of a deuteron beam of final energy 40 MeV computed at an equilibrium orbit radius of 20.351" using the measured electric and magnetic field data. The two figures, corresponding to displacements from the equilibrium orbit, precess in the directions shown by the arrow heads and close on themselves after 62 turns.

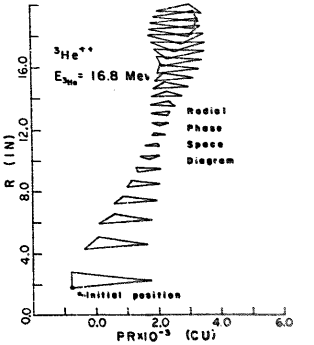

Fig. 14. A radial phase-space plot for a $^3He^{++}$ beam of final energy 16.8 MeV. The ions, starting with the initial position shown (the ion source), become centered at a radius near 12". See text for explanation.

it reaches the extraction radius. The program ORBIT has been used to calculate the trajectory in radial phase space of the accelerated ions as a function of the initial conditions. A typical example for 16.8 MeV $^3He^{++}$ is shown in fig. 14. The three points representing the vertices of each triangle are determined by sampling each 120° for one turn without energy gain. They represent therefore three points on the radial phase-space ellipse separated by one-third of a precessional period. Thus the area of the triangle is an approximate measure of the radial phase-space oscillation amplitude. The ion is then accelerated through one half turn and a new triangle computed. For an accelerated beam centered at extraction, the area of the triangles will shrink monotonically with radius, with the vertices coinciding at extraction. By iterating the initial trajectory of the ions, the optimum position of the ion source with respect to the cyclotron center (the offset) can be readily optimized to $\pm\frac{1}{8}$". The ion source offset calculated in this way agrees well with the simplified calculation given by eq. (11).

At small radii where the flutter is necessarily small, a central magnetic bump is used to increase the vertical focusing. As a result there is a transition region between the central radially decreasing field and the increasing isochronous field (about 8"–10" in radius) where $n = 0$ and, as indicated by eq. (5), a resonance exists for first harmonics. The sensitivity of the orbits in this region is exploited by using the harmonic coils to compensate for any existing or equivalent first harmonic at these and smaller radii. To estimate the magnitude of first harmonic required, the program ORBIT was altered to include two independent magnetic first harmonics of arbitrary radial extent, phase, and amplitude. One harmonic was used to induce a radial oscillation in the beam, and the second was then adjusted to minimize the oscillation at large radii. It was known from the magnetic field measurements that the first harmonic component of the field was less than 5 G, and estimates indicated that the equivalent magnetic first harmonic due to electric field asymmetries was less than 10 G for a reasonably well-centered beam. Based on the calculations, the harmonic coils were designed to produce a first harmonic component up to 30 G over the radial range from 8" to 12" and adjustable in azimuth.

Their effect on the centering of orbits is demonstrated by the phase-space plots in fig. 15, calculated for 29 MeV D^+. At a radius of 11" the amplitudes of radial oscillation vary by two orders of magnitude and are of opposite phase.

5.4. Phase selection

The requirement of single turn extraction places a stringent requirement on the phase width of the accelerated beam. Ions are extracted from the ion source over a

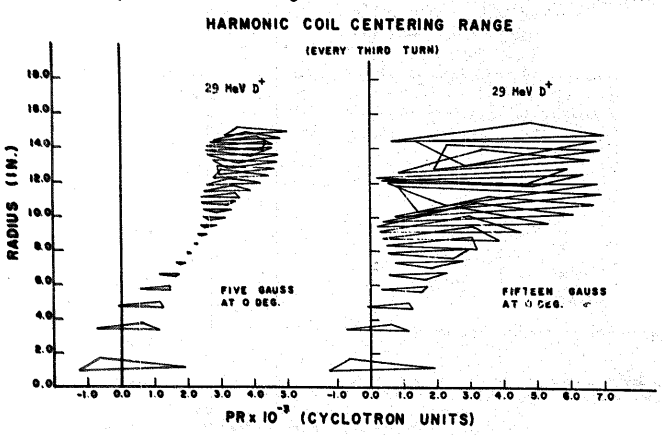

Fig. 15. Radial phase-space plots demonstrating the effect of the harmonic coils on a deuteron beam of 29 MeV final energy.

wide range in phase and since their energy gain is a function of phase, there is no one value of the tower offset that will lead to centering for all ions. To prevent precessional mixing it is necessary to limit the phase acceptance. The limit, assuming the magnetic field is isochronous and the ions nonrelativistic, is set by the condition that the range in R_n given by an initial phase width $+\phi_0$ centered on $\phi = 0°$ be less than the turn spacing. Since

$$R_n = \frac{1}{\omega_c}(4nqV_D \cos\phi/m)^{\frac{1}{2}},$$

and the spacing between adjacent turns is

$$\Delta R = \frac{1}{\omega_c}\frac{\Delta E}{\sqrt{(2E)m}}, \text{ or } \frac{\Delta R}{R} = \frac{1}{2}\frac{\Delta E}{E}, \qquad (12)$$

then

$$\phi_0 \leqslant \cos^{-1}\left(1 - \frac{1}{n}\right).$$

For ions making 200 turns, this implies an upper limit of $\phi_0 \leq 6°$.

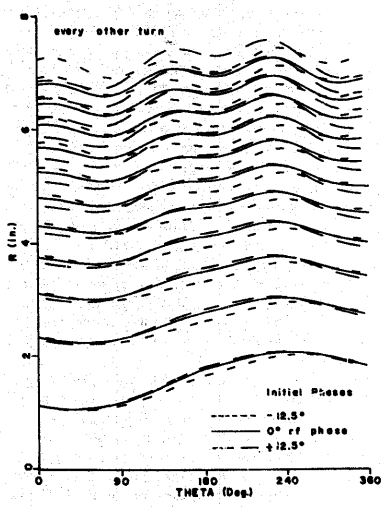

Fig. 16. Trajectories of the early orbits for three ions emerging from the ion source in the same initial direction but at rf phases of 0° and ±12.5°. Only every other turn is plotted.

To determine the optimum position in the cyclotron at which to limit the phase width, the trajectories of ions emerging from the ion source in the same initial direction but at an rf phase of 0° and ±12.5° were computed. The results for 45 MeV $^3He^{++}$ are shown in fig. 16. The largest radial separation of the three trajectories occurs on the first few turns at an azimuth near 180° as expected since the magnetic field is essentially flat near the center and thus acts as a uniform field spectrometer for which the focus occurs at 180° in azimuth. While ions of different energy are dispersed in radius, unfortunately the distribution is double-valued in θ, except at $\theta_0 = 0$. Since

$$\frac{\Delta\theta}{\Delta R} = \frac{B(qV\cos\theta)^{\frac{1}{2}}}{V\sin\theta},$$

the phase width for a given radial increment will be widest at $\theta = 0°$. Further, uncorrelated effects such as the finite size of the source make a narrow phase selection at zero degrees essentially impossible with the normal ion source. The gated ion source, however, has two unique characteristics that permit efficient and narrow phase selection at the first half turn.

The first characteristic is the restriction in geometry due to the addition of the control and screen electrode, which cuts off ions with leading rf phase in excess of about 20°. Thus for phases lagging by 20° or more, the correlation becomes one to one. It is worth noting that $\Delta\theta/\Delta R$ decreases as the phase lag increases, and therefore the phase selection becomes more effective.

The second characteristic is that, unlike the conventional ion source for which the current extracted from the plasma is proportional to the three-halves power of the dee voltage, the current from the gated source is independent of dee voltage. The current per unit phase width is thus a constant, independent of phase, and intensity is not sacrificed when a lagging phase is selected. Since a magnetic bump is used in the central region to provide vertical focusing, the initial lagging phase can quickly be brought to zero by adjusting the magnitude of the bump to the appropriate value. Thus with the gated ion source, phase widths of the order of a few degrees can be routinely obtained. A slit adjustable both in width and radial position, located at 190° in azimuth and on the first half turn in radius, is used to select both the initial phase and phase width.

5.5. Axial motion

Small asymmetries in the electric field in the central region can give rise to large-amplitude vertical

oscillations. Because there is no effective damping mechanism (adiabatic damping is relatively small), the oscillation will persist to extraction. In the region of $\nu_r = \omega_r/\omega_0 = 1$, before the flutter has taken over, the vertical restoring force is weak and beam may be lost. Typical values for ω_z are $0.1\omega_0$ to $0.2\omega_0$, so that the vertical motion when observed at a fixed azimuth has a period of the order of 5–10 turns. Thus if the amplitude is large, the difference in vertical position between two successive turns may also be large. In particular, the extracted beam may show considerable z-motion as the one turn more or less is made in the cyclotron, and this motion is reflected in the z-position of the beam in the external ion-optical system. The z-motion was investigated using the burn-pattern technique. The oscillation can be suppressed[18]) by a pair of "suppressor" plates. The plates are 1" wide (in azimuth) and extend 2" in radius. They are located near the center of the cyclotron, where the turn spacing is still large, so that they only act on one or two turns. They are placed one above and the other below the median plane, and a potential difference of up to ±600 V and balanced to ground is applied. They are positioned in azimuth and radius such that the total impulse applied to the ions at the instant they pass through $z = 0$ is equal and opposite to their z-momentum. Their effectiveness is shown in fig. 17. Note that the period of the vertical motion varies between 5 and 8 turns as expected.

5.6. The extraction problem

It was known at the time of the original design and construction of the cyclotron that for the two-dee system, ions accelerated at 0° rf phase would experience, at the instant of extraction, an rf voltage in the deflector channel lagging by 60° and in opposition to the applied dc voltage, thus requiring a higher dc voltage to extract the ions. It was also understood[1])

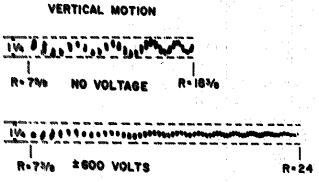

Fig. 17. Burn-patterns of the z-motion showing the effectiveness of the suppressor plates. The large z-amplitude in the top pattern is nearly eliminated by the suppressor field as shown by the bottom pattern.

that, depending on the phase width of the beam, the rf would fan out the beam and increase the radial emittance, and the aperture of the external beam-handling system was increased accordingly. The point that was overlooked was that the rf voltage on the deflector, unlike the dc voltage, increases the energy spread of the beam since it adds a velocity or momentum component in quadrature, the magnitude of which depends on both the phase and phase width of the beam appearing at the septum and on the effective electrical length of the deflector channel. It was expected that by removing this contribution to the energy spread, the intensity of beam in the scattering chamber for a given quality would be increased by a factor of 2–5. The loss in energy gain per turn was not considered serious because the dee voltage could be increased. It was for this reason that the conversion to a-one-dee system was made in 1972.

The improvement is demonstrated by the results obtained for 11.4 MeV deuterons. (This low energy was chosen for study because the number of turns to extraction could be varied easily by more than a factor of two and because the relatively small radial gradient and resulting lower radial stability limit provided a more sensitive indication of the presence of any residual first harmonic.) Using the emittance snooper probe, the radial emittance was measured to be 3.1 mm mrad for 50% of the beam, with an effective source width of 0.20 mm. The extraction efficiency was about 85%, and of the extracted beam essentially 100% appeared at the image surface of the first of the two beam preparation magnets. This is to be compared with earlier measurements for a 15 MeV deuteron beam which gave an emittance of 24 mm mrad for 30% of the beam with an effective source width of 0.51 mm and an extraction efficiency of 75% with only 30% of the extracted beam appearing at the focus of the first beam preparation magnet (FM1). Normalizing the emittance measured for 11.4 MeV deuterons to 15 MeV, the radial emittance of 2.7 mm mrad for 50% of the beam is to be compared with 24 mm mrad for 30% of the beam.

To determine the limits on the radial position and radial momentum of the ions at the entrance of the extractor channel that will result in successful extraction, a slightly modified version of the computer program ORBIT was used to track ions through the channel and into the first beam preparation magnet (fig. 22). The septum is located in radius at 36.56" just inside the $\nu_r = 1$ region where the isochronous field turns over, and well inside the Walkinshaw resonance ($\nu_r = 2\nu_z$). Thus the ions available for extraction are

those presented to the extractor from the intermediate region. Fig. 18 shows the radial phase-space history of the last three turns prior to extraction of a 40 MeV D^+ beam. The shaded areas represent the region of space from which, according to the code EXTRACTOR, beam may be extracted. Superimposed on the figure are the phase-space plots for ions undergoing radial oscillations. It is apparent that only the ions on full-energy orbit will extract from the equilibrium orbit. Ions from other turns will be extracted only when they have the amplitude and phase of radial oscillation that meet the criterion for extraction.

Using the program EXTRACTOR, the trajectories of ions differing in initial conditions are tracked through the extractor channel and magnetic fringe field to the magnetic field-free region. Those rays falling within the acceptance limits of FM1 when extrapolated back upstream give the radial position and radial phase-space density, hence the radial width and angular divergence of the effective source accepted by the external ion-optical system, Calculations were carried out for a variety of geometries of the extractor channel to determine the optimum position and length. The electric field in the channel, and hence the voltage required for extraction, is a function of the position in azimuth of the septum and the length of the channel. Because of the threefold symmetry of the magnetic field, the radial momentum of the ions varies with azimuth and this puts an additional constraint on the allowable position of the septum. On the basis of the computer calculations, the extractor channel was lengthened and shaped, and the septum moved in azimuth from 240° to 225°. The change resulted in a 15%–20% reduction in the required extraction voltage.

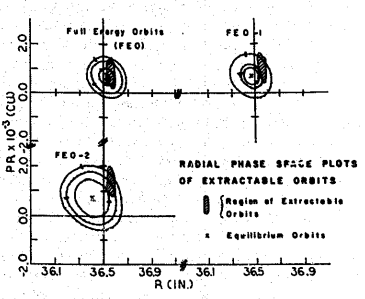

Fig. 18. The radial phase-space regions of extractable orbits for 40 MeV deuterons.

While the extraction efficiency has proved adequate, it is possible to improve it, particularly at higher energies by means of a "pre-extractor", the purpose of which is to increase the turn separation at the septum. It consists of a pair of parallel plates about 6" long, 35° upstream from the septum to which a radial dc electric field is applied. While this will not reduce the required extraction voltage, it should increase the turn separation at the septum by a factor of two. The pre-extractor has been built but is yet to be tested.

The carbon septum* slides into grooves into the leading edge of the extractor and may be easily replaced. The deflector bar is oil-cooled and operated at voltages from 20 to 90 kV depending on the ion species and energy. [The required electric field in the channel is $E = (2T/q)(\Delta\rho/\rho^2)$, where ρ is the radius of curvature and $\Delta\rho$ the required change in radius.]

Deflector power supply and regulator. The power supply for the deflector, manufactured by Kilovolt Corporation, is rated at 120 kV and 30 mA. Because the output is unregulated and has approximately 1% ripple, an external series regulator has been added. Filter capacitors are to be avoided because of the stored energy dumped in the discharge from deflector to ground. The negative output voltage is sampled through an oil-cooled 225 MΩ resistor and summed with a dc reference voltage. The sum signal passes through an amplifier of dc gain 106 dB and bandwidth 0.01 Hz. The amplifier drives a series tube, type 4PR400A, in the positive ground return side of the supply. Since the rated maximum voltage for this tube is 20 kV, suitable relay logic controls the input variac to the supply to keep the voltage within operating range. Under normal operating conditions the beam presents only a small loading (less than 100 μA) on the supply so that a 15 MΩ load is placed across the load inside the oil tank. A series resistor of 15 MΩ is used for output voltages greater than 60 kV to limit sparking current through the deflector bar. Because current

* Originally tungsten was used as the septum material. Sometime after ^{3}He beams began to be used, a high level of low-energy contamination was discovered inside the main vacuum chamber of the cyclotron. This was determined to be due primarily to 70 d and 170 d activities of ^{183}Re and ^{184}Re, respectively, and was being produced by ^{3}He bombardment of the tungsten septum. As a result a study was made of suitable septum materials. Plates machined to 2" × 10" × 0.018" from Ultra Carbon F-purity graphite have been found to increase the septum life by a factor of five and at the same time eliminate the contamination problem. There is, however, some evidence that carbon sputtered from the septum onto the extractor bar tends to reduce the effective break-down voltage.

fluctuations due to small discharges produce an *IR* drop in the resistor, it is jumpered out for the lower voltages.

The stability of the regulator has been checked with a digital voltmeter for long-term variations and a Tektronix high-voltage probe for ripple modulations. Ripple on the output is less than 25 V peak to peak and the long-term stability is better than $1/10^4$. The effect of a variation in deflector voltage on the stability of the extracted beam was studied in connection with the neutron time-of-flight system and is described in section 5.8.

5.7. Tuning

In the original two-dee design it was planned to operate the cyclotron with constant-turn geometry. However, with the reduced energy gain per turn with one dee, it is now operated more nearly in a constant dee-voltage mode and the central geometry is changed as required. The advantages of operating at maximum energy gain per turn are obvious and follow from the discussion of the preceding sections. Because the central geometry is frequently changed, it is essential that there be a systematic method of tuning quality beams. With the diagnostic probes available, this has become a straightforward and relatively quick task. The procedure described below is that followed when ions are to be accelerated to an energy not previously used. Beams which have been run can, of course, be tuned more quickly since the settings are known.

The dee voltage is typically 45–50 kV. The position of the tower, puller, and phase-selection slit are calculated and set accordingly. The gradient coil currents to provide the isochronous field for the particular particle and energy are calculated using the computer program. With the phase slit retracted and the integral current probe set at a small radius ($\approx$ 10″–15″), the ion source is adjusted in position and roll with respect to the puller to optimize the beam.

The phase probe is then used to determine the rf phase and the phase width of the accelerated beam and to confirm that the magnetic field is isochronous. During tuning the ion source is gated on every rf cycle and the stop signal scaled down to occur every other rf cycle. In this way the beam generates two time signals which are exactly one rf period apart. The TAC output of the phase probe is fed into a multichannel analyzer, and the analyzer calibrated in degrees per channel. The channel corresponding to zero degrees rf phase is determined using the following technique. With the centerline probe placed at some radius near extraction, the main magnet is raised until the γ-ray signal from the beam just disappears. This implies that the beam is at virtually 90° leading phase. The main magnet is then lowered until again the beam just disappears corresponding to 90° lagging phase. Zero phase is presumed to have been located when the difference in channel number corresponds to 180°. If a difference of 180° is not obtained, it can be concluded that the beam was cut off because of phase excursions at a smaller radius. In this case the inner gradient coils are adjusted to increase the acceptance, and the process is repeated until a 180° spread is achieved.

The phase width of the beam is adjusted by means of the opening and positioning of the phase-defining slit located on the first half turn. (Normally the slit is moved through the turn toward the machine center in steps and the phase width at each point measured.) A phase history of the beam is then plotted from a radius of about 15″ to extraction, and any small adjustments of the gradient coil currents necessary to achieve isochronism throughout this range are made with the aid of fig. 3 using an iterative process. When the field is isochronous, the absolute phase of the beam can be shifted by a slight change of an inner gradient coil until the beam rides at zero phase out to extraction. Typically the field is trimmed to an accuracy of $\pm 4°$, but with care the deviations from 0° can be made less than 2° over the range from 15″ to extraction. Such fine adjustments are made only after the centering process is completed.

The orbits are centered using the information supplied by the turn pattern. If the amplitude A of the radial oscillation is large, the central geometry must be corrected. The tower, puller, and the phase slit are all moved along the dee gap in such a way as to keep the same phase width and absolute phase. By taking turn patterns at a number of positions, the phase of the radial oscillation can be made to shift by 180° and an optimum position can be determined. It is not necessary to adjust the geometry precisely since fine control of the centering process is afforded by the harmonic coils. Once an acceptable tower position has been located, a series of turn patterns is taken as a function of harmonic coil amplitude and azimuth. A wide variation in centering can be attained with these coils. With the centroid of the beam current centered, the phase of the turn-width modulation is adjusted to minimize the turn width at the septum. Since the turns are focused at any given azimuth twice per normal precessional period and since the period is typically 40–50 turns, changing the number of turns by 12 at the most is sufficient to minimize the width of the last few turns. This change is most simply accomplished with a

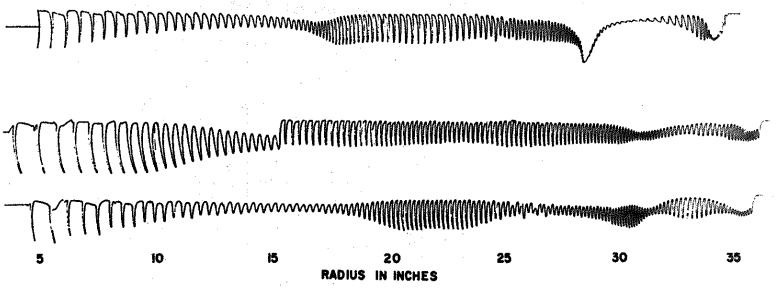

Fig. 19. Turn patterns for an 11 MeV deuteron beam. The top pattern is typical of an uncentered beam. The lower pattern demonstrates turn-width modulation. The middle pattern demonstrates the effect on turn-width modulation of the divergence slit located at a radius of 16". A radial oscillation of small amplitude between 30" and 35" is still evident in the middle pattern. Top, middle and lower pattern are referred to in the text as a, b, and c, respectively.

slight change of the dee voltage. These last adjustments are easily made with the beam gated at, say, *f*/6. By stopping the phase probe TAC at the gating frequency, beam from different turns striking the same object may be distinguished. When the γ-rays produced by the extracted beam striking the centerline probe all arrive at the same rf period, single-turn extraction has been achieved. The phase probe, of course, also monitors the beam during the tuning process and detects beam striking anywhere other than the centerline probe, such as the dee lips, indicating vertical blow-up. It is also useful in following the beam down the extractor channel as the deflector voltage is raised and in adjusting the channel position.

Three typical turn patterns (current density vs radius) for an 11 MeV deuteron beam are shown in fig. 19. As described in section 5.1, for a centered beam the areas under each turn should be equal and the spacing between turns decrease as $1/R$, as in fig. 19b. Fig. 19a is typical of an uncentered beam. The normal turn spacing is modulated at a period corresponding to the precessional frequency ω_p, and where the amplitude of the radial oscillation becomes large, the individual turns overlap to produce a "bump" like that at a radius of 31". While the pattern of fig. 19b represents a reasonably well centered beam since the individual turns are distinguishable throughout the pattern, a small radial oscillation exists as is indicated by the compression and expansion in spacing at 31" and 33", respectively. The modulation of the turn width, evident in fig. 19c, has been limited in fig. 19b by the divergence slit located at a radius of 16". The slit is particularly useful during the tuning process since, as discussed earlier, the turn width modulation can obscure information about the turn spacing. The effect of the harmonic coils on the beam is demonstrated by the four short patterns of fig. 20.

Additional information is contained in the differential current measurements. For example, the area under each turn will remain constant if no ions are lost to the beam. (It will, in fact, decrease slightly with radius when the range of particles becomes comparable to the wire radius.) The height of a bump is a direct measure of the number of overlapping turns, and the variation in $R\Delta R$ with radius is a sensitive measure of centering. The effective dee voltage can be calibrated

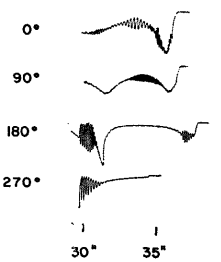

Fig. 20. Four turn patterns demonstrating the effect of the harmonic coil phase.

from the turn spacing since

$$V = 2.64\times 10^{-4}\frac{f^2 A}{2nN}(R_2^2 - R_1^2), \qquad (13)$$

where n is the number of turns between radii R_1 and R_2, A is the atomic mass, N is the charge state, f is in MHz, and R is in inches. If the ions ride at zero phase between R_1 and R_2, then V is the dee voltage in kV. Because the adiabatic damping is small, the minimum turn width should be $w = s + \delta r$, where s is the width of the phase slit (or the divergence slit), and $\delta r = R(1 - \cos\theta)^{\frac{1}{2}}$. Any additional increase would normally indicate a modulation in the dee voltage, rf frequency, or the magnetic field.

5.8. Stability

The requirements of high-resolution charged-particle spectroscopy on the one hand and high-resolution time-of-flight measurements on the other, set definite but different requirements on the stability of the dee voltage, frequency, and magnetic field. Time of flight requires single-turn extraction while high-resolution measurements require a fixed source position[19]) and an energy stability of $1{:}10^4$. As will be evident from the discussion below, the stability in energy requires the dee voltage to be stable to the order of $1{:}10^4$ and the rf frequency and magnetic field to $1{:}4\times 10^4$.

The stability requirement imposed by single-turn extraction can be obtained from the equation for the energy at extraction (assuming centered orbits); namely, it is the sum of the energy gains on all of the n turns on the way to the septum.

$$E_n = \sum_{i=1}^{n} 2qV\cos(\theta_i), \qquad (14)$$

where θ_i is the phase on the ith turn, q is the ion charge, and V is the dee voltage. The only variables on the right-hand side are the dee voltage and the phase. The phase will reflect any fluctuations in either the magnetic field or the frequency.

A fractional change in the dee voltage, $\Delta V/V$, will be reflected directly in the energy of the nth turn, that is

$$\frac{\Delta E_n}{E_n} = \frac{\Delta V}{V}.$$

The fractional change in E_n due to a fluctuation in the magnetic field (or the frequency) can be obtained as follows. Consider a small change ΔB in the magnetic field B. Since

$$\omega = \frac{qB}{m},$$

it follows that

$$\frac{\Delta B}{B} = \frac{\Delta\omega}{\omega} = -\frac{\Delta T}{T}.$$

Thus the change in B causes a change in the phase on each turn. (A change $\Delta f/f$ in the rf frequency f would have exactly the same kind of effect as $\Delta B/B$) If ΔB is small and $\theta_0 = 0°$, then the energy after n turns can be written

$$E_n + \Delta E_n = \sum_{i=1}^{n} 2qV\cos(2\pi i\,\Delta B/B)$$

$$= \sum_{i=1}^{n} 2qV[1 - \tfrac{1}{2}(2\pi i\,\Delta B/B)^2].$$

The series can be summed to yield

$$E_n + \Delta E_n = 2qV[n - \tfrac{1}{6}n(n+1)(2n+1)\,2\pi^2(\Delta B/B)^2].$$

Without the fluctuation, $E_n = 2qVn$; thus the fractional change in the energy after n turns can be identified in terms of ΔB as

$$\frac{\Delta E_n}{E_n} = -\tfrac{1}{3}(n+1)(2n+1)\,2\pi^2(\Delta B/B)^2. \qquad (15)$$

The sensitivity of E_n to dee voltage or field fluctuations can be estimated. If an ion ordinarily takes n turns to receive its final energy, then it will require $n+1$ turns if the dee voltage drops by a fractional amount $1/n$. That is

$$\frac{\Delta E_n}{E_n} = \frac{\Delta V}{V} = \frac{1}{n}.$$

To obtain the fractional change in B or f required to produce the same effect, set $\Delta E_n/E_n$ equal to $1/n$ in eq. (15). The result is

$$\frac{\Delta f}{f} = \frac{\Delta B}{B} = \left(\frac{3}{2\pi^2 n(n+1)(2n+1)}\right)^{\frac{1}{2}} \approx \frac{1}{n^2\pi}.$$

Thus the energy of the nth turn is more sensitive to changes in B than in V. However, this is not enough information to set the limits on the stability. The requirements for single-turn extraction are that it not be possible to get parts of two different turns extracted and onto the target. For a reasonably centered beam the condition required to allow extraction is simply that the beam clear the inside of the septum on one turn

and be outside it on the next. It should be noted here then that the energy spread accepted by the extraction channel is only limited by the turn spacing. That spacing is determined by the dee voltage and the phase and final energy of the ions.

Consider an ion which just misses the inside of the septum on the nth turn and is extracted on the $(n+1)$th turn. If the energy of the nth turn increases enough to cause the radius to increase by the thickness of the septum, the ion will be extracted one turn earlier. Thus the stability limit for single-turn extraction is given by by the fluctuation which will cause this radial change in the nth turn. Since $E \propto R^2$

$$\frac{\Delta R}{R} = \frac{1}{2}\frac{\Delta E}{E}.$$

The septum radius is about 90 cm and the septum thickness is of the order of 0.030 cm; $\Delta R/R$ must then be less than 1/3000 and $\Delta E/E$ less than 1/1500. These criteria were found for the special case where the nth turn just missed the septum. If the turn consisted only of ions of the same phase and if the radial extent of the beam due to the ion source emittance were negligible, then the average stability requirements would not be this stringent. In practice, however, the turn width due to phase and emittance effects is often comparable to the turn spacing, so that the sensitivity to fluctuations is maximized and well represented by the limiting case discussed above. For example, for a beam that makes 200 turns to extraction, the energy change between the 200th and 201th turns is 1/200. If the phase width is 6° and the absolute phase is only 2° off zero, then the energy spread in one turn will be 0.75/200. Thus the radial spread will be three-fourths of the turn spacing.

If the energy variation is to be kept to 1/1500, the dee voltage must be stable to 1/1500. Then, from eq. (15), assuming 200 turns, $\Delta f/f$ must be less than about 1/3000. This is not the case for $\Delta B/B$. Because the radius is a function of both E and B, a change in B will affect the radius of the nth turn in two ways. For example, if the beam is initially riding at zero phase, then an increase or a decrease in B will cause a decrease in E_n and therefore in the radius. But the radius associated with any given energy will increase in the first case and decrease in the second. Assuming the ions are initially at zero phase, the change in energy ΔE_n of the nth turn for a particular $\Delta B/B$ can be found from eq. (15) for a given value of E_n, n, and $\Delta B/B$. The radius of the nth turn is

$$R_n = \frac{(2mE_n)^{\frac{1}{2}}}{qB}.$$

The change, ΔR_n, in R_n induced by a change in B can be computed using

$$R_n + \Delta R_n = \frac{[2m(E_n - \Delta E_n)]^{\frac{1}{2}}}{q(B \pm \Delta B)}.$$

If n is 200 and the magnitude of $\Delta B/B$ is taken as 1/3000, then $\Delta R_n/R_n$ is 1/1500 if ΔB is positive and virtually zero if ΔB is negative. Thus the two effects are comparable in magnitude. Since they add under certain conditions, the effective limit on $\Delta B/B$ is 1/6000, a factor of two more stringent than the limit on $\Delta f/f$.

It is noted here that when the cyclotron is being used for a charged-particle experiment all ions that enter the extraction channel will be available for processing on the basis of their energy alone regardless of the number of turns made inside the cyclotron. Since the resolving power is typically $1/10^4$, to optimize the intensity of the beam on target, it is desirable to hold the energy to this tolerance. Thus from the discussion above, the requirements on $\Delta V/V$ and $\Delta f/f$ (or $\Delta B/B$) are $1/10^4$ and $1/4 \times 10^4$, respectively (assuming $n \approx 200$).

Stability measurements. The rf frequency may easily be held to $< 1/10^6$. The stability of the dee voltage and the magnetic field may be divided into two time domains, short (<30 ms) and long. Long-term instability is due mainly to drifts in reference voltages or to thermal effects, such as expansion or contraction of the dee structure and resonator. It has been measured in a variety of ways. In one, the differential current probe is positioned on the slope of a single, well defined turn near extraction, and the fluctuations in the ratio of current to the differential probe to the total current is measured for long periods. This method is capable of measuring variations in the dee voltage and/or the magnetic field to $1/10^4$. In a second method, the same in principle as the first, the current probe is positioned just at the extraction radius so that half the current of a single turn is intercepted on the centerline probe and half on the septum. The time variation of the ratio of prompt γ-rays produced at these places is also a measure of the stability of the dee voltage and/or magnetic field. The results of such measurements are consistent with a long-term stability in the dee voltage of $1/10^4$, in the magnetic field of a few parts in 10^5, and an intensity of the order of 1%. It was by such measurements that fluctuations due to the stepping motor in the dee tuning system and the cycling of the cooling tower water were discovered.

Still another measure of the long-term stability

comes from the measurement of the phase and phase width. With the ion source gated, say, at $f/6$, the centerline probe is adjusted in radius near extraction to intercept only the leading part (in radius) of a given turn. If the field is accurately isochronous and if the beam is at 0°, those ions in a narrow phase width ($\approx 2°$) at 0° will be intercepted. The remaining ions consisting of both leading and lagging phase make one additional turn before striking the probe. The time distribution observed with the phase probe, therefore, is that plotted in fig. 21, which is a plot from the multichannel analyzer. This is convincing evidence of narrow pulses of ions stable in phase and radius.

Short-term stability, particularly effects correlated with the 60 Hz line frequency, were also investigated using the phase probe. With the beam gated at the source and intercepted on the centerline probe at some radius as described above, the prompt γ-rays detected by the phase probe indicate the fraction of the beam striking the probe in one turn or the next. This time-of-flight spectrum is stored in a two-dimensional array in coincidence with a signal generated by a 60 Hz ramp. If the beam is being swept from turn to turn by a fluctuation synchronized with 60 Hz (or 120 Hz or 360 Hz), then the magnitude and frequency of the effect can be observed directly in an isometric display of the data. The sensitivity of the technique is related to the absolute phase and the phase width of the beam, as discussed above. With this technique, a malfunction in the dee-voltage regulation system of $1/10^3$ was discovered. Regulation now is better than $1/10^4$. The frequency stability of the master oscillator is rated at $1/10^8$, while the magnetic field is stable to less than $1/10^5$. Results from the two-parameter diagnostic set-up are consistent with these values.

After the correction was made to the dee-voltage regulator, the time width, the intensity, and the gating efficiency of the extracted beam were found to be modulated at frequencies of 60 Hz, 120 Hz, and 360 Hz; the intensity was also modulated at a frequency of the order of 700 kHz. The 700 kHz component has been attributed to oscillations of the plasma within the ion source, and while they result in some loss of intensity, they do not appear to affect the beam quality, which suggests space-charge effects are not significant. The 60 Hz related modulations were more serious in that the beam intensity was modulated as much as 100% with a 50% duty cycle and in addition increased the time width of the time-of-flight beam pulse by as much as 1 ns.

The modulation was traced to two sources, 60 Hz pick-up in the time reference signal and ripple in the deflector power supply. Ground loop pick-up in the time reference signal obtained from the dee voltage caused a modulation in the flight times measured by the phase probe. Ripple in the output of the regulated dc extractor voltage can change the trajectory of the ions through the extractor channel and thus the arrival time of the beam on target. This modulation has since been reduced to less than 0.03%. The sensitivity of the diagnostic probes to modulation was calibrated by injecting into the dee voltage, ion source and deflector regulator a 100 Hz modulation of known amplitude and observing the results with the phase probe in a two-dimensional count-rate versus time spectrum. This technique provided a convenient diagnostic tool to sort out which systems were responsible for the time modulations on the external beam.

6. External ion-optics

The floor plan of the cyclotron facility is shown in fig. 22. The beam after extraction from the cyclotron can be directed to either the high or low resolution beam lines by switching on or off magnet FM1. The instrumentation for measuring the emittance of the extracted beam, the snooper E1 and wire scanning probe E2, are located as shown on the plan. The quadrupole doublet Q1 is used only with the low-resolution line.

6.1. The high-resolution line

Designed primarily for charged-particle spectroscopy with a resolving power $E/\Delta E = 8 \times 10^3$, the basic design and constructional details of the beam preparation system and reaction-products analysis system have

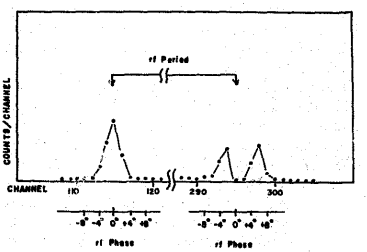

Fig. 21. The time distribution of a pulse of 20 MeV $^3He^+$ ions striking the centerline probe. Those near 0° rf phase extend to larger radius and are intercepted by the probe on one turn; the remaining ions must make one additional turn to reach the radius of the probe.

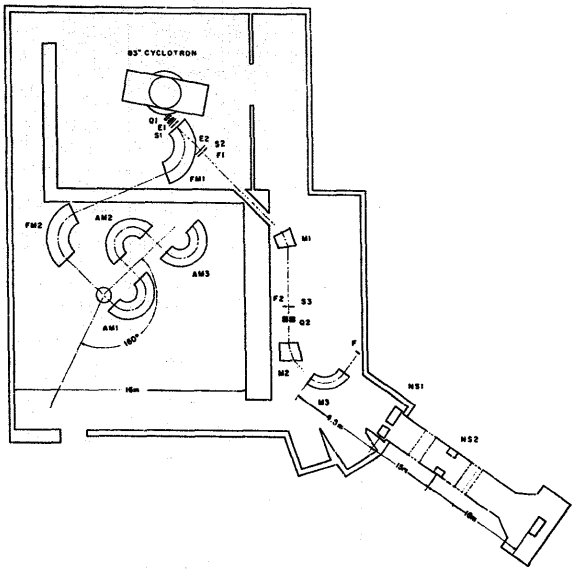

Fig. 22. Floor plan of the cyclotron facility. Not shown are the (α, xny) and charged-particle stations following the switching magnet M2. The neutron detectors are normally located at the end of the tunnel in the lower right-hand corner of the figure.

been described in detail previously[1]).

The beam preparation system consists of two outside "C" magnets, FM1 and FM2, each of wedge angle 110°, $n = \frac{1}{2}$, and 200 cm radius of curvature. These parameters result in equal image and object distances of 350 cm and a dispersion at 40 MeV of 10 keV/mm for each magnet and therefore 5 keV/mm for the two magnets in series. The useful aperture is 2" high by 6½" wide and results in a solid angle of 4×10^{-4} sr. The vertical acceptance angle is 0.65°, and the radial acceptance angle is 2.1°. Each magnet contains 26 t of steel, 5700 lbs of copper, and requires 7.5×10^4 ampere-turns to provide a field of 8000 G.

The power supply (35 kW) for each magnet is a three-phase reactor-controlled unit rated for 135 V at 260 A. The magnetic field regulator is similar to that of the main magnet; the current and magnetic field are held constant by one regulator loop while the voltage drop across a series transistor panel is held within the proper range by a reactor driver. The current sensor is a water-cooled constantan shunt which produces 5 V for a current of 260 A. The current signal provides for short-term regulation while long-term feedback is obtained from an NMR device. The sensor signals are summed with a stable Zener reference at the input of an amplifier with a dc gain of 150 dB and a bandwidth of 0.005 Hz. The regulator drives the series transistor panel consisting of 30 parallel 2N173 transistors. The panel is designed to operate at an average voltage drop of 9 V or power dissipation of 2.4 kW. The short-term stability is measured by observing the ripple voltage across the magnet. The main contribution is 40 mV of 60 Hz which produces a field variation of less than $1{:}10^6$. The long-term stability is determined by the NMR device and is better than $1{:}10^5$.

The reaction-products analysis system consists of three 180°, $n = \frac{1}{2}$ magnets of radii of curvature 133 cm (AM1, AM2, AM3). The principal parameters are:

image and object distance = 93 cm, solid angle $= 4 \times 10^{-4}$ sr, dispersion = 15 keV/mm per magnet at 40 MeV or 5 keV/mm for the three in series. Each magnet weights 33 t and the system of three can be rotated in angle about an axis through the target from $-10°$ to $+180°$ with respect to the direction of the beam on the target, maintaining the axis of rotation fixed to better than 0.002". The ion-optics are described in detail in ref. 1.

The power supplies and regulators for each of the three magnets are similar to those of the focusing magnets except the supplies are rated for 120 V at 400 A. The constantan shunts produce 5 V at 400 A and the transistor panels consist of 45 parallel 2N173 transistors. The feedback and reference voltage are summed at the input of a high-gain two-stage amplifier. The amplifiers have a dc gain of 150 dB and an initial breakpoint at 0.001 Hz. At 8 Hz the response is leveled out to 76 dB until a final breakpoint at 50 kHz. This gives a larger gain at higher frequencies and results in an improved response to line-voltage transients. The stability of the magnetic fields is again better than $1{:}10^5$.

Questions of source emittance and line shape, line shape and resolution, determination of image surfaces and aberrations, resolution and brightness, dispersion cancellation, kinematic corrections, detectors, momentum matching, calibration and precision Q-value measurements have been discussed in detail previously[19,20]).

Typical currents to the scattering chamber are 75–100 nA per $E/\Delta E = 10^4$ for singly ionized ions and 40–50 nA for doubly ionized. As described in ref. 19 an additional factor of ten in intensity can be obtained without loss in resolution using dispersion cancellation.

6.2. The low-resolution line

Designed for neutron time-of-flight measurements, a variety of charged-particle measurements such as (α, xn), (α, γ), lifetime measurements, and for the low-resolution study of heavy-ion induced reactions, the ion-optical system has a resolving power of $E/\Delta E = 10^3$. The details of the ion-optics and the time-of-flight spectrometer are described elsewhere[14]). Typical currents are 1 μA of singly ionized ions for $E/\Delta E = 10^3$. By relaxing the single-turn extraction requirement and accepting a larger energy spread, beams up to 5 μA have been obtained.

The beam line incorporates five magnets. The two quadrupole doublets (Q1 and Q2) and two of the three dipole magnets (M1 and M2) were purchased from Alpha Scientific (model no. 3014 and 3021 quadrupoles and model no. 3095CB dipoles). Each is powered with regulated supplies furnished by Alpha Scientific, and the two dipole magnets are field-stabilized by an NMR also supplied by Alpha Scientific.

The neutron target magnet (M3) was constructed originally as an inside "C" uniform field 90° reaction products analyzer for use with the 50" cyclotron. It has been converted to an outside "C" for use with the neutron time-of-flight system. The target is moved in azimuth through the gap to change the scattering angle between the incident beam and the detectors (D) at the end of the neutron tunnel. The slits NS1 and NS2 are adjusted horizontally to match the target position.

The magnet is powered by a reactor-controlled, series-regulated supply similar to those in the high-resolution line. The regulator amplifier is chopper-stabilized with a dc gain of 140 dB. Because the stability requirement is only $1{:}10^4$, no magnetic field sensor is used in the feedback path.

Over the years many people have contributed to bringing the cyclotron facility to its present state. A number of students, former and present, have contributed hours of time to tedious jobs, such as field measurements. We would particularly thank A. S. Broad for his effort in modifying the ion source for the one-dee configuration and D. A. Lewis for his assistance in the orbit studies effort. The laboratory owes a tremendous debt to W. E. Downer who, with the assistance of J. Koenig, M. W. Prince, D. Schleede, and A. V. Smith, has been responsible for all the mechanical, constructional, and operational aspects of the facility. Their efforts have exceeded the norm by far.

References

1) W. C. Parkinson, R. S. Tickle, P. Bruinsma, J. Bardwick and J. M. Lambert, Nucl. Instr. and Meth. **18**, **19** (1962) 93.
2) R. S. Livingston and R. J. Jones, Rev. Sci. Instr. **25** (1954) 552.
3) R. H. Day and W. C. Parkinson, Nucl. Instr. and Meth. **111** (1973) 199.
4) R. H. Dishington, Elec. Engng, **67** (1948) 1043.
5) A. Papineau, P. Benezech and R. Maillard, J. Phys. Rad. **21** (1960) 410.
6) See, for example, IEEE Trans. Nucl. Sci. NS-**19** (1972).
7) M. L. Mallory, E. D. Hudson and G. Fuchs, IEEE Trans. Nucl. Sci. NS-**19** (1972) 118.
8) M. L. Mallory and H. G. Blosser, IEEE Trans. Nucl. Sci, NS-**13** (1966)163.
9) T. A. Welton, NAS-NRC 656 (1959) p. 192 (Proc. Conf. on *Sector-focused cyclotrons*; Sea Island, Ga., Feb. 1959); H. G. Blosser and M. M. Gordon, Nucl. Instr. and Meth. **13**

(1961) 101; K. R. Mackenzie, Nucl. Instr. and Meth. **31** (1964) 139; M. Reiser, IEEE Trans. Nucl. Sci. NS-13 (1966) 171; see also Nucl. Instr. and Meth. **18, 19** (1962) 370; M. M. Gordon, Proc. 5th Intern. Cyclotron Conf., Harwell 1969 (Butterworth, London, 1971) p. 305; S. Holm, Nucl. Instr. and Meth. **64** (1968) 317.

10) L. H. Thomas, Phys. Rev. **54** (1938) 580.

11) The six volumes of the Proc. Intern. Cyclotron Conf. contain a wealth of material and indicate the progress made over the past two decades.

12) K. R. Symon, D. W. Kerst, L. W. Jones, L. J. Laslett and K. M. Terwilliger, Phys. Rev. **103** (1956) 1837.

13) H. G. Blosser, IEEE Trans. Nucl. Sci. NS-13 (1966) 1.

14) W. C. Parkinson, J. F. Petersen, R. H. Day, R. M. Polichar, P. F. Julien and D. C. DuPlantis, submitted to Nucl. Instr. and Meth.

15) H. A. Grunder, F. B. Selph and H. Atterling, CERN 63-19 (1963) p. 59.

16) D. J. Clark, Harwell Cyclotron Design Note No. CDN-500-05-024 (Rutherford Laboratory, Harwell, England, Aug. 28, 1962).

17) This is not the two-gap crossing resonance discussed by M. M. Gordon Nucl. Instr. and Meth. **18, 19** (1962) 268.

18) W. C. Parkinson, W. S. Gray, J. F. Petersen and R. H. Day, AIP Conf. Proc. #9 (Cyclotrons–1972) p. 366.

19) W. C. Parkinson and J. Bardwick, Nucl. Instr. and Meth. **78** (1970) 245.

20) W. C. Parkinson, *Atomic masses and fundamental constants* (Eds. J. H. Sanders and A. H. Wapstra; Plenum Press, 1972) vol. 4, p. 38.